Development of Water Simulation System for Ultrasonic Detection of Inclusions in Molten Metals

Yuanbei Zhang

A Thesis
in
The Department
of
Mechanical & Industrial Engineering

Presented in Partial Fulfillment of the Requirements
for the Degree of Master of Applied Science at
Concordia University
Montreal, Quebec, Canada

August 2003

Your file Votre référence
ISBN: 0-612-83892-7
Our file Notre référence
ISBN: 0-612-83892-7

ABSTRACT

Development of Water Simulation System for Ultrasonic Detection of Inclusions in Molten Metals

Yuanbei Zhang

In metal processing, metal cleanliness is a crucial process parameter for product manufacturing and recycling and, therefore, on-line ultrasonic methods to evaluate the cleanliness of molten metals are highly desired. In order to establish a procedure and to investigate the optimum system configurations, a water simulation system of ultrasonic detection has been constructed in this thesis. Measuring the concentrations, counting the numbers and measuring the size distributions of the polyvinyl chloride (PVC) particles in water is performed with the ultrasonic pitch-catch configuration. Ultrasonic signals scattered by the particles are detected and the single particle movement is successfully identified. This study verifies that the water simulation system can be employed to evaluate the cleanliness in water.

Ultrasonic probes directly associated to the system sensitivity are crucial for ultrasonic techniques. In this thesis, several materials and shapes of metallic buffer rods are investigated experimentally using an ultrasonic longitudinal wave transducer (UT). Furthermore, the ultrasonic wave patterns of different cross-section shapes of rods are investigated by scanning a small ball bearing immersed in water with pitch-catch mode. Finally, evaluation and recommendations for the application of these high performance metallic buffer rods is presented in this thesis.

ACKNOWLEDGEMENTS

I would like to thank the Lord for His initiation, provision, and direction in my studies. As well, I would like to thank my wife Chunyan, my dear parents and my sisters for their endless care, encouragement, and support throughout my years of study.

I also want to thank my thesis supervisor, Prof. C.Y. Su for his love and the energy he put into recommending that I study this project, his continual encouragement, and financial support.

Next, I want to thank my thesis supervisor, Dr. C.-K. Jen. Without his guidance, care, and help, this work would not have been possible. From him, I have learned about ultrasonic techniques in an environment where a research ethic of the highest level prevails. His approach has allowed me to extend what I've learned to life in general.

I also wish to express my sincere gratitude to my thesis supervisor, Dr. Yuu Ono for his guidance in this study directly, and for the time he spent being an excellent mentor. Through his dedicated efforts I have learned a lot; not only technical knowledge, but also diligence and a strict scientific approach.

I would like also to acknowledge the contribution of Mr. J.F. Moisan and Mr. C. Corbeil for their technical support with the equipment installation. Many thanks to Mr.

Harold Hebert for his implementation of the Labview program. Thanks to Dr. Z.G. Sun, Mr. J. Yan and Mr. D.H. Zhao for their sincere assistance.

Finally, I would like to gratefully acknowledge the financial support from the National Research Council of Canada (NRC), especially its Industrial Materials Institute of Boucherville (IMI) where all the experiments were carried out.

TABLE OF CONTENTS

LIST OF FIGURES

LIST OF TABLES

Chapter 1: Introduction

1.1 Background

Seeking to produce improved and consistent products efficiently has been a high preoccupation in manufacturing industries. Several factors determine the quality of products made of metals, such as the amount of elements traced, dissolved gas content, and non-metallic inclusions. Inclusions inside melt often lead to impaired mechanical properties of metals. Some examples of the defects caused by inclusions are, deterioration of the surface quality in rolled or extruded products and fractures in drawn wires. Additionally, the presence of inclusions may cause porosity and corrosion of the metals. As a result, inclusion detection and removal technologies have been developed, such as electromagnetic sedimentation, filtration, and flotation in degassing units, etc. These methods have been successful in removing inclusions as an integrated part of the continuous casting process, but they have limitations. The sedimentation method takes time and cannot completely remove all the impurities in the melt. Also, in this method, any handling or movement of the filters can send inclusions trapped in the mesh of the filter into the production line. Thus, the development of simple and reliable techniques and equipment to monitor and control melt quality is essential.

At present, vast applications of metals, particularly the lightweight metals such as aluminum (Al) and magnesium (Mg), have resulted in a large amount of casting scrap.

Due to both economic and environmental concerns, the scrap must be recycled, and the metals to be recycled usually contain a high level of inclusions. In order to produce high-quality recycled metals, the characterization of inclusions in molten metal, such as amount, size, particle conductivity, and shape must be well identified, efficient, and economical. For these reasons, techniques for assessing the cleanliness of the melt are required.

Until now, there have been various conventional techniques available to evaluate metal quality. These techniques can be classified into two main groups: off-line methods such as sampler tests and filtration techniques, and on line methods such as the Liquid Metal Cleanliness Analyzer (LiMCA) and ultrasonic techniques. Off-line methods, normally based on extraction of a metal sample followed by analysis in a laboratory, are capable of providing the desired information regarding inclusion content. However, they require considerable sample preparation and analysis time and the information is always obtained too late to be fed back to the process. Ideally, evaluation of the cleanliness of molten metals would be conducted on large quantities, which could rapidly be analyzed with little or no sample preparation. This can only be achieved by analyzing the metal while it is still in the molten state. For molten Al processing, the LiMCA is commonly used and accepted. However, the LiMCA is not yet applicable to other molten metals. In addition, it is not capable of effectively detecting conductive inclusions, such as metallic particles, which are often present in molten Al and Mg. Furthermore, if the particle is larger than the orifice diameter of the system, the orifice will be blocked and must be

replaced. Therefore, because of these deficiencies, there is a need to develop advanced or alternative techniques for the inclusion detection in molten metals.

Ultrasound, due to its capability of probing inside materials nondestructively, is widely used to monitor and control processes as well as to evaluate materials and products in various industries. The desirable features of ultrasonic technique signals are (a) on-line measurement, (b) rapid response, usually a fraction of a second, (c) excellent long-term stability and reliability, (d) low power consumption and (e) high spatial resolution [1]. Parallel to the LiMCA development, ultrasonic techniques have been reported as on-line methods to monitor the liquid metal properties [2-8]. However, ultrasonic techniques for assessing the inclusions in liquid metals are still not used industrially. These techniques are still under development because the sensor's stability, repeatability, and sensitivity at high temperatures are not sufficiently evaluated for inclusions in molten metal.

There are three primary objectives in this thesis. The first objective is not only to improve the sensor's performance but also to reduce the cost of machining sensors. The second objective is to design, build and test a water simulation system, in which the feasibility of the ultrasonic approach as an on-line metal cleanliness analyzer will be investigated. This series of experiments includes measuring the inclusion concentration, counting the number of particles, and determining the size of the particles. The third objective is to apply the procedure developed in the water simulation system to the

evaluation of cleanliness using molten magnesium as an example, so that the ultrasonic method can be tested in a real environment.

1.2 Molten Metal Cleanliness Evaluation

1.2.1 Inclusions in Metals

Lightweight metals such as aluminum and magnesium have gained much acceptance in structure applications and are widely used in the automotive, electronic, transport and aerospace industries. In order to produce high-quality products of such lightweight metals, developing a metal cleanliness evaluation system is important during molten metal processing. The objective of the cleanliness analyzer is to identify the characteristics of inclusions such as the size, shape, type, and distribution of inclusions.

In the case of aluminum (Al), the impurities can be oxide films such as corundum (Al_2O_3) and Spinel ($MgAl_2O_4$), and Al_2O_3 particles, together with hard carbide inclusions (Al_4C_3 and SiC) derived from the original melting process. Corundum films are in the range of 10 to 5000 μm and are either suspended on the liquid surface or trapped within it due to the turbulence of the melt. In the case of Spinel, its size range is from 0.1 to 100 μm. For the Al_2O_3 particle, the range of size is from 0.2 to 30 μm. The ranges of the hard carbides inclusions, Al_4C_3 and SiC vary from about 0.5 to 25 μm and 0.5 to 5 μm, respectively [9-10].

The magnesium (Mg) industry has similar problems. Liquid Mg oxidizes in the protective atmosphere during the primary manufacturing steps leading to a large variety of inclusions being introduced into the melt. The inclusion contents in magnesium are 10 to 20 times higher than that of aluminum [11]. The composition of inclusions in magnesium is more complicated, and can be classified into two groups. The non-metallic inclusions group includes magnesium oxide and nitride particles in the range of 10 to 300 μm, Na, Ca, Mg and K-based chloride particles in the size range of 10 to 50 μm. The other group might be aluminum and calcium-based carbides (Al_4C_3 and CaC_2); and magnesium-based sulfide (MgS), fluoride (MgF_2), and sulfate ($MgSO_4$). The second category, called the metallic inclusions group consists of iron-rich particles in the range of 0.5 to 10 μm. Also, there are 0.5 to 1 μm thick, and 50 to 400 μm long oxide/nitride films in the molten magnesium [12-14].

Inclusions in Al and Mg melts will provide us with the range of the particle sizes we will be detecting. Therefore, the ultrasonic system under development in the thesis needs to detect a range of sizes from less than 1 μm up to 5000 μm in order to successfully monitor all the inclusions mentioned above.

1.2.2 Conventional Methods

In order to achieve high quality recycled metals, the characteristics of inclusions need to be well identified, the particles inside the metals must be effectively quantified at the molten stage during processing, and more advanced techniques for evaluating the

cleanliness of the metal must be developed. At present, several techniques are currently available for assessing the content of inclusions in molten metal. These techniques can be categorized into four main groups: filtration techniques, fracture tests, LiMCA, and ultrasonic techniques.

Until now, filtration techniques have been divided into two groups: vacuum-filtration and pressure-filtration. The Union Carbide tester and the porous disc filtration analysis (PoDFA) are typical examples of them, respectively. In these two off-line methods, molten metal passes through a filter. When solidification is achieved, the counting and analyzing of inclusions begin. Filtration techniques are being widely applied in aluminum and steel industries due to the following merits: (a) filtration can be carried out directly in the bulk molten metal at any location; (b) it can offer useful information on the chemistry and shape of inclusion and (c) the cost is low in comparison to other techniques. Another off-line method of measurement of cleanliness is the fracture-test technique. It is based on the extraction of a metal sample followed by analysis of inclusions in the laboratory after solidification. A typical application of this technique is the K-Mold device. This technique has the same advantages as the filtration technique does. However, all off-line techniques have the common disadvantages: (a) they require considerable sample preparation and analysis time to discover possible molten metal processing problems (b) the information obtained is often too late to make a rapid control adjustment in the production process, and (c) the data collected from the solidified metal differs from that collected from it in its molten state. Thus, the ability of

a technique to measure and monitor metal cleanliness continuously in the liquid state is highly desired [15].

In the Al industry, a common on-line detection technique is the LiMCA (Liquid Metal Cleanliness Analyzer) [16-17]. This system includes the probe, current source, and signal processing system. In the probe, a constant current is maintained between two immersed electrodes. They are separated by a tube with a small orifice in its wall. When a particle passes through the orifice, the resistance increases in direct proportion to a particle's volume and the voltage between the electrodes changes. Based on this electrical sensing zone principle, particles can be detected. Since the middle of the 1980's, the LiMCA has become a commercially available tool for on-line measuring the total concentration and size distribution of inclusions in aluminum industries. Now its detection capability of particle size in liquid Al is from 20 to 300 μm (LiMCA II) [18]. The LiMCA has distinct merits. However, there are still limitations with this instrument: (a) it is difficult to detect metallic inclusions effectively, (b) the orifice is easily blocked by the large particles, (c) the amount of liquid to be tested at a time is limited, (d) the cost of operation is high, and (e) the applications for other metals is under development although reports state that the application of the LiMCA has been extended to steel, cast iron and copper [19-21].

1.2.3 Ultrasonic Techniques

The ultrasonic techniques can be used in molten metal cleanliness due to their unique features, as mentioned earlier. These techniques have been applied to detect both nonmetallic and metallic inclusions for many kinds of metals, and even for identifying the shape and size of the inclusions. The basic operation principle of ultrasonic detection is as follows: a signal generated by a transmitting ultrasonic transducer (UT) is sent into the liquid metal. In the liquid metal, a part of the signal energy reflects when ultrasonic waves encounter inclusions and a receiving UT then receives the reflected signal. Generally, there are three kinds of modes based on sensors' configuration: transmission, pulse-echo and pitch-catch mode (see Fig. 2.2.). The details will be explained in Chapter 2. In each mode, the received ultrasound signal carries the information about velocity (time delay) and attenuation (amplitude) of the desired signal to be measured because ultrasonic propagation characteristics such as velocity and attenuation in the liquid may be changed owing to the energy scattered from the inclusions present in the liquid metals. The scattered ultrasonic signal may reveal the characteristic of the inclusions. In detail, the ultrasonic signals include not only the geometric size of the inclusions and their population density, but also the ultrasonic impedance of inclusions. Thus, ultrasonic sensors or sensor systems for monitoring and analyzing the inclusions in liquid metals may have potential advantages compared to the LIMCA and off-line methods.

Applying ultrasonic techniques to detect inclusion in liquid metal started in the 1950's. N.D.G. Mountford and R. Calvert [22] did the experiments with a pulsed

ultrasonic technique to investigate the precipitation in liquid aluminum alloys at the Rolls Royce Foundry, Derby, England and demonstrated the feasibility of the basic principles. Since then a new field of application of ultrasonic techniques for metal cleanliness has opened up. Recently many researchers have joined the investigation and invented various methods and systems [2-8].

Research into ultrasonic techniques employed in this area have become increasingly more complete leading to improved function of the techniques and the development of ultrasonic systems with a high sensitivity for detecting the size and quantity of particles. One typical example was Reynolds 4MTM system made by T. L. Mansfield. Researchers reported that particles larger than 100 μm were detected in molten Al and steel [23-24].

In the earlier studies [25-29], researchers used non-cladding probes operating in pitch-catch mode to evaluate molten Al, however, the sensor's sensitivity was not sufficient for application in industry. From the late 1980's, enhanced attention was focused on the improvement of the performance of the buffer rod probes. Since then the signal-to-noise-ration (SNR) of probe has been greatly improved. In 1987, C. K. Jen reported a new and improved buffer rod (ultrasonic probe) with a pure copper core and a pure aluminum cladding [30]. In their later works, C. K. Jen *et al.* improved probes not only in clad technique, but also in the geometry of the rod [31-32]. It was these crucial improvements that pushed forward the application of ultrasonic technique in metal cleanliness.

At present, owing to the increase of SNR of the ultrasonic probe, it is possible for ultrasonic techniques to be used for many practical applications. Such techniques have been successfully applied not only to molten Al, but also to Mg and other metals such as liquid zinc, sodium and steel [33-34]. Also, they have been applied for the in-line monitoring of metal die casting processes [35-36] and polymer processes [37-39].

So far, there are several applications of ultrasonic measurement techniques in manufacturing industries. Ultrasonic sensors are widely accepted and used for level and flow measurements. However, ultrasonic techniques for monitoring cleanliness of liquid metals are still under development and not commercialized yet.

1.3 Ultrasonic Buffer Rods

On-line ultrasonic monitoring during manufacturing processes is often performed under elevated temperatures and high pressures, e.g. over 700 ^{0}C for Al industries. Although high temperature piezoelectric transducers (UTs) are commercially supplied by several companies: Etalon (Lizton, Indiana), Ultran (Boalsburg, PA), Ishikawajima Inspection and Instrumentation Co. LTD (IIICL, Tokyo, Japan) and RTD (German), etc, they are not suitable for inclusion detection in liquid Al and Mg due to insufficient workable temperature, SNR, bandwidth, and strength. It is also difficult to find a high performance ultrasonic couplant at elevated temperatures. Therefore, an alternative approach to monitor the inclusions is to use ultrasonic buffer rods. The probing end of the rod is

inserted into the molten metal while the other end contacting UT is air cooled to room temperature. This method allows the use of conventional UTs and commercial ultrasonic couplants.

In the buffer rod probe, due to the diffraction of ultrasound, the mode conversion of longitudinal wave to shear wave and the reverse happens at the rod periphery. Therefore, trailing echoes appear in the rod as undesired noises and signal-to-noise-ratio (SNR) of the probe decreases. . The SNR is defined as the amplitude of the desired signal at the rod end over that of the noise produced in the rod. This SNR relates to the detection sensitivity directly: the higher the SNR, the better the sensitivity. In attempting to develop improved ultrasonic systems for monitoring metal cleanliness, selecting the correct buffer rods is critical [40-41].

The challenging issues facing the investigation of buffer rods are (1) collecting information about the acoustic properties in materials, (2) ultrasonic transmission and reflection at the interface of media, (3) reducing the noise during ultrasonic measurements (4) the attenuation of sound increasing with frequency, (5) maintaining the relationship between ultrasonic performance and high temperature. In summary, the research [42-45] may be divided into three main and interrelated categories:

(a) Materials: Attenuation in ultrasonic propagation is crucial for the material selection. For example, large grain sizes in steel normally induce more scattering losses reducing the signal strength, increasing the noise and thus greatly deteriorating the SNR.

An important criterion for choosing probe materials is balancing the wetting and corrosion of materials [46-48]. Wetting and corrosion are two phenomena normally in conflict: wetting at the probing end that is inside the liquid metal is desirable because in this way ultrasonic energy can be efficiently transmitted into molten metal, however, wetting induces corrosion and degrades the buffer rod which limits the time of the on-line measurement. The corrosion is also associated with the system's long-term stability of operation. For the reasons mentioned above, researchers have been devoting time and effort in choosing suitable materials for probes [40].

(b) Cladding technique: Clad buffer rods consisting of a core and a cladding have superior ultrasonic performance over non-clad rods. The ultrasonic waves are guided into these clad buffer rods by a method similar to the one used in guiding optical waves into a clad optical fiber, i.e. the energy is concentrated and well guided in the core. The design rules of clad buffer rods are: (1) the velocity of the core should be different from that of the cladding and this difference can be even higher than 20%, (2) the acoustic impedance of the core should be close to that of the cladding. Two techniques, namely, thermal spray [41] and electroplating [42], can be used to fabricate the cladding of buffer rods. Reports state that these cladding buffer rods having a high SNR have made many practical applications feasible [31, 40].

(c) Shape of probe: The shape of the probe will affect the signal strength and SNR. Reports have been published illustrating various probe shapes, such as tapered rods with different slopes, spiral boundary covered rods, etc [32, 44, 47]. Thus, in order

to attain a higher SNR and signal strength, making use of non-symmetric geometry in the lateral plane and axial direction of the probe to reduce trailing echoes will produce good results. As well, fabricating a lens at the end of the probe can enhance the spatial resolution and the capability to detect small particles [43, 45, 46].

In [40], various core and cladding materials, such as steel, stainless steel, zirconium, titanium, nickel, copper and aluminum, buffer rods were fabricated by thermal spray techniques. Comparisons on ultrasonic performance between non-clad and clad buffer rods were reported. All experimental measurement results showed good SNR in these clad buffer rods. For example, the ultrasonic measurement of a 6.35 mm diameter and 125 mm long clad zirconium (Zr) rod with 1.2 mm thick stainless steel cladding, using a 10 MHz longitudinal UT, showed that the trailing echoes were significantly eliminated and the signal strength of main echo was 8 dB stronger than that of non-clad Zr rod having the same diameter and length. A tapered buffer rod can reduce unwanted spurious echoes effectively. In [47], it has been experimentally verified that the amplitudes of trailing echoes were gradually reduced as the tapering angle increased up to 2.0^0. Buffer rods having ultrasonic lens at the probing end were applied to V (z) measurement to obtain velocity of leaky waves [51] and C-scan imaging [43, 52] of the sample immersed in molten zinc and aluminum.

In this thesis, Al was chosen as buffer rod material because it can be easily machined to the desired testing geometries. In addition, when the Al rod is employed in water simulation, the reflection coefficient at the interface of the rod and the water is only

0.16. This lower reflection coefficient level assures that the sensitivity of detection particles in molten metals is expected to be better than that in the water . The cross-section shape of buffer rods will be designed in Chapter 3 as square, rectangle and circle in order to evaluate the SNR and signal strength. Furthermore, for comparison purposes, one group of buffer rods will be clad with stainless steel, and another group will be kept without cladding. The SNR of each buffer rod will be tested with UTs having different shapes (circle and square) and different ultrasonic operating frequencies (5 MHz and 10 MHz). Finally, after comparing the results, the best combination of the buffer rod and the UT will be chosen for further water simulation experiments.

1.4 Thesis Content

1.4.1 Objective

The task of this thesis is to develop a water simulation system for the ultrasonic evaluation of molten metal cleanliness. We will establish the procedure, investigate the optimum system configurations and evaluate sensitivity, accuracy, inspection volume, and speed for measuring sizes and counting the number of inclusions.

1.4.2 Content

Chapter 2 introduces several basic ultrasonic concepts in order to give a background and to explain terminology. The data acquisition system of ultrasonic measurement will be introduced.

Chapter 3 introduces a series of tests for buffer rods with different materials and shapes, where the performance of each buffer rod will be evaluated by comparing the SNR and signal strength of each probe.

Chapter 4 presents the design, construction, and test results of the water simulation system for ultrasonic detection of PVC particles in water. The detection capacity of this system such as measuring particle concentration, counting the number and measuring the size of particles will be demonstrated.

Chapter 5 describes the preliminary experiments for evaluation of Mg cleanliness in the melt pool based on the study with the water simulation system. Experimental results of inclusion detection and relative cleanliness evaluation in molten Mg will be presented.

Chapter 6 summarizes the thesis, presents the conclusions, and proposes recommendations for potential improvement and future research studies.

Chapter 2: Ultrasonic Techniques and Data Acquisition System

2.1 Basic Ultrasonic Theories

2.1.1 Introduction

Ultrasonics is the science and exploitation of elastic waves in solids, liquids, and gases, which have frequencies greater than 20 kHz. With the help of ultrasonic wave propagation, ultrasound can be used for the characterization of materials and in-line process monitoring [53]. Ultrasonic techniques have some significant advantages such as non-destructive testing (no damage to the material), non-intrusive inspection (no disturbance to or interference with the process), fast response, and low cost. Being an excellent tool for in-line or on-line monitoring, ultrasonic methods have been used extensively in manufacturing industries since the 1940s. Advances in electronics and computer power, leading to new signal acquisition and processing, made applications to the precise measurement of ultrasound for a variety of purposes possible. The basic principle of ultrasonic measurements is that an ultrasonic transducer (UT) generates ultrasonic waves that transmit into the material, traverse inside the material and are received by the same or another UT. The received ultrasonic signals carry the information about the properties of the material. In ultrasonic measurements, parameters, such as the reflection coefficient at the interface, the ultrasonic velocity and attenuation in the material, and scattered signals in the material, are commonly measured as a function

of ultrasonic frequency at different operation conditions. The measured ultrasonic parameters can be correlated to material properties (such as viscosity, density, composition, grain size, thickness, and Young's and shear modulus) and subsurface defects, voids (location, size, shape, and distribution), and process conditions (temperature and pressure) [53].

All the ultrasonic parameters are obtained from the ultrasonic signals. The propagation of some specific features of the signals can be measured with increasing accuracy. There are two classes of measurable features: time delay and amplitude. The time delay is the propagating time of ultrasonic waves and is a very useful feature. For example, when the wave-speed is known, the path length can be calculated by the time delay. The path length allows accurate measurement of distance e.g., thickness, internal dimensions and location of inclusions. The amplitude of a wave can be used to determine the damping (energy absorption) characteristics of the material, thereby indicating the material properties. These two important features dominate the applications of ultrasonic techniques [1, 53].

2.1.2 Signal to Noise Ratio (SNR)

Ultrasonic signal to noise ratio is defined as the strength of the desired echo divided by that of the undesired ones. SNR represents the dynamic range, which is crucial for material evaluation and characterization. The inclusion detection sensitivity investigated in this study is directly related to this SNR. When the SNR is higher, the detection

sensitivity is better. The undesired signals in this study mainly come from electric noise emitted by the electric devices and spurious echoes created in the buffer rods employed. We will focus on discussing the latter case because it is the main source of noise.

The well-known result of using a long buffer rod is the presence of spurious echoes due to mode conversion, wave reverberation and diffraction within the rod of finite diameter and specific shape, and scattering echoes from random grains or the voids in the rod materials. The unwanted spurious signals, especially the trailing echoes [54], affect SNR significantly in the ultrasonic measurements. Fig. 2.1 shows a typical ultrasonic signal measurement for a buffer rod test in pulse-echo mode. The UT is attached to one end of the buffer rod. The first echo L^1 represents the longitudinal ultrasonic wave reflected from the other end of the buffer rod. L^n denotes the *n*th round trip longitudinal wave echo in the rod. However, one can see that there are many other signals between the L^1 and L^2 echoes. If this buffer rod is applied for particle detection and the desired signals reflected from the particles appear between L^1 and L^2, the undesired signals will interfere with the desired signals. In Fig. 2.1, these unwanted signals are called trailing echoes. In order to improve the SNR of the measurement, two approaches are attempted in this study: (1) controlling the shape of the buffer rod to reduce the trailing echoes; (2) adjusting the alignment of rods to avoid the detected signals appearing at the locations of trailing echoes. More details will be given later.

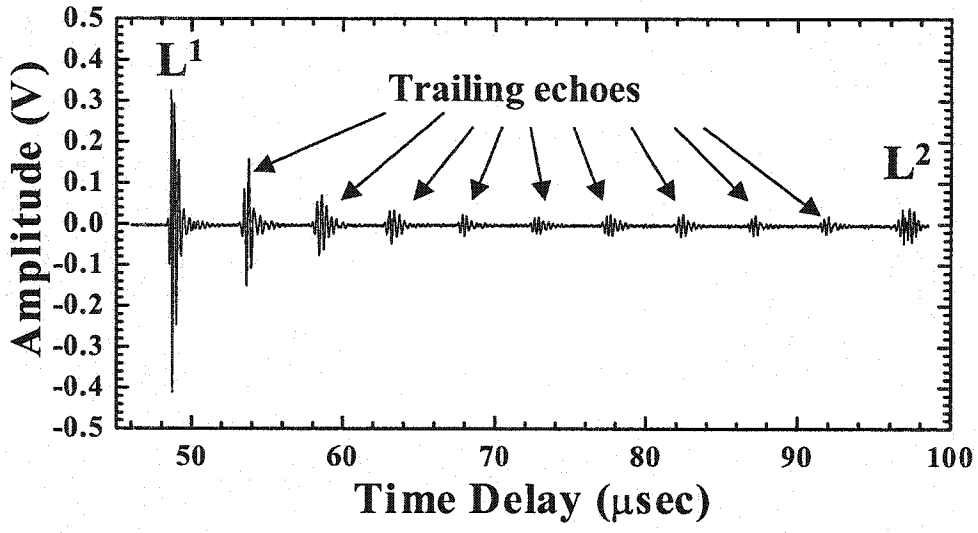

Fig. 2.1: A typical ultrasonic signal measured with a buffer rod in pulse-echo mode.

2.1.3 Ultrasonic Measurement Configurations

As mentioned earlier, ultrasonic waves can be generated by a UT and received by the same UT or another UT in the measurements. Commonly used sensing configurations are transmission, pitch-catch and pulse-echo modes, as shown in Fig. 2.2. In Fig. 2.2, "T" denotes a transmitter while "R", a receiver. For the transmission mode, as shown in Fig.2.2 (a), two UTs are set at two-sides of the sample. The ultrasonic waves propagate from "T" to "R" directly and single trip inside the material gives less energy loss. This configuration is suitable for measuring the thickness of samples. However, for some on-line ultrasonic monitoring applications, this configuration is not convenient because it requires a two-side access to the UTs at specific locations. Also it is not practical for our

particle detection. In the pulse-echo mode, the signal is transmitted and received by a single UT, as shown in Fig.2.2 (b). This mode is preferred in some applications because it can save the space of installing probe and only one side access is required. The last configuration is pitch-catch mode. As shown in Fig. 2.2 (c), two UTs are used with an angle. It has better SNR than the pulse-echo mode for the ultrasonic measurements using buffer rods, since the path of the first reflected signal (L^1) is the shortest one. The undesired signals will reach the receiving UT later than the desired signal. Fig. 2.3 shows the comparison of ultrasonic measurements in the pulse-echo mode (left) and the pitch-catch mode (right) with buffer rods. One can see that the desired echo is clearer due to the better SNR in the pitch-catch mode than in the pulse-echo mode. Therefore, the pitch-catch configuration is used for particle detection experiments in this study.

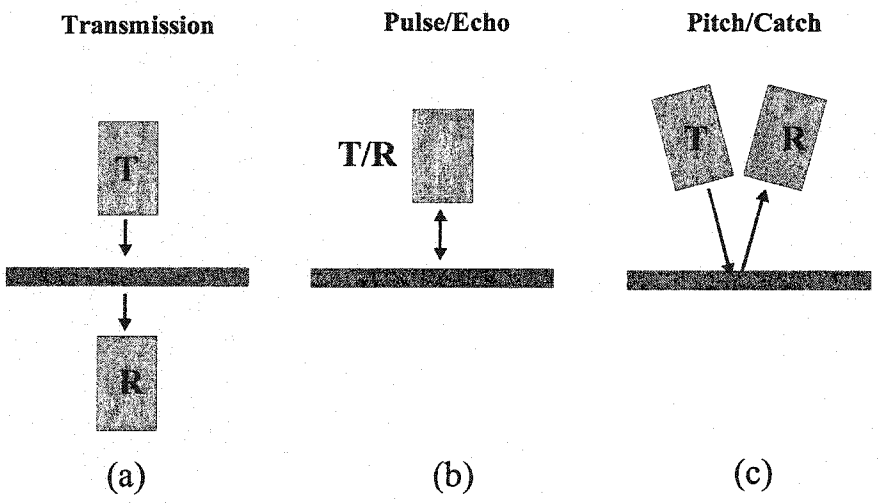

Fig.2.2: Commonly used sensing configurations.

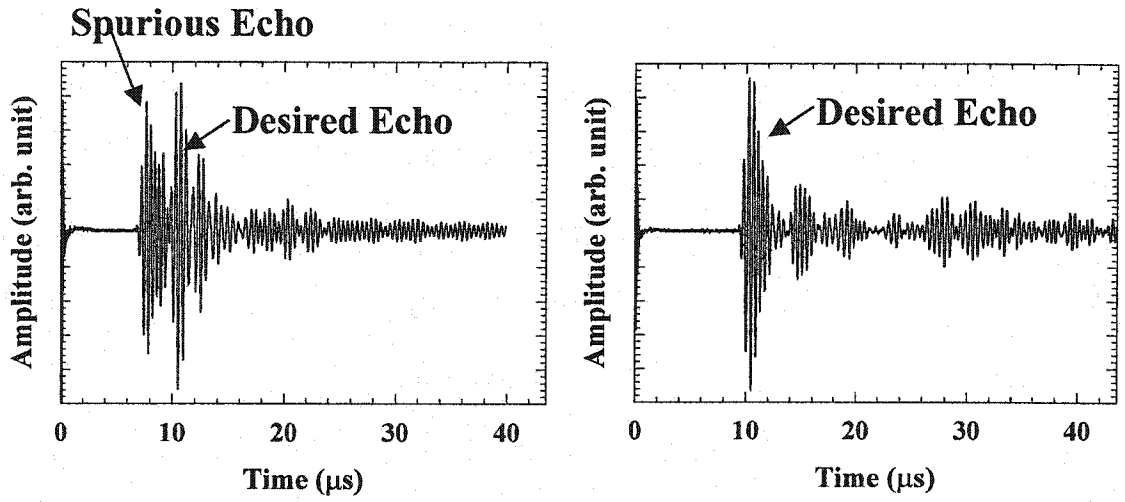

Fig. 2.3: The comparison of ultrasonic measurements in pulse-echo mode (left) and pitch-catch mode (right).

2.1.4 Reflection and Transmission coefficient

When a plane wave impinges on an interface between two materials having different properties, this wave will be separated into two waves: one, called a reflected wave, will be reflected back to the first medium, and the other, called a transmitted wave, will be transmitted into the second medium. The directions of these waves obey Snell's Law. The amplitude of the reflected wave is used for the calculation of the reflection coefficient and that of the transmitted wave is used for the calculation of the transmission coefficient. The expressions of the reflection coefficient (R) and transmission coefficient (T) can be defined as the following equations [55]:

$$R = \frac{Z_2 - Z_1}{Z_2 + Z_1} \tag{2-1}$$

$$T = 2\frac{Z_2}{Z_1 + Z_2} = 1 - R \tag{2-2}$$

where the subscripts, 1 and 2, represent the first and the second mediums, respectively, and Z is the acoustical impedance of the medium, which is defined as the product of the density, ρ , of the medium and the wave velocity, v, in the medium.

The reflection and transmission coefficients need to be considered when choosing buffer rod materials, which will be discussed further in Chapter 3.

2.1.5 Ultrasonic Attenuation

When a uniform ultrasonic plane wave propagates in a material, the amplitude (or power) of the wave will decrease due to propagation attenuation. The attenuation occurs due to diffraction, scattering, and absorption. Amplitude of ultrasound, A, can be expressed as the function of propagation distance x:

$$A(x) = A_0 e^{-\alpha x} \tag{2-3}$$

where A_0 is an initial amplitude, α is an attenuation coefficient measured in nepers per meter [N_p/m].

Another common measured unit called decibel (dB) is expressed as:

$$ATT(dB) = 20\log\ (A/A_0) = -20\alpha x \log e = -8.868\alpha x \tag{2-4}$$

Since log (1/2) = -0.3010, an attenuation ratio of 1/2 is close to –6dB, which is often referred value. In other words, the meaning of 6 dB down is that the amplitude changes to half.

2.1.6 Scattering

The interaction of a wave with a nonuniformity produces reflections and transmissions in multiple directions, called scattered waves [56]. The magnitude of scattering waves depends on space derivatives of the elastic properties and on the density of the solid. After scattering, constructive interference creates a wave that propagates in the same direction as the incident wave, called the forward scattered wave. The wave pattern propagating backward toward the source is called the backscatter. The study, [56-58], states that when the wavelength of a incident wave is small compared to the sphere diameter, most of the incident wave is reflected as backscatter, with little refraction in the direction of propagation. When the wavelength is large, the reflection is diminished by interference between the waves but the transmission is enhanced considerably into a forward scattered beam. Typical scatter patterns for a single sphere are illustrated in Fig. 2.4 [56]. In our particle detection, the backscatter waves are useful to characterize the particle. Scattering is required to choose the suitable ultrasonic frequency for determining particle sizes.

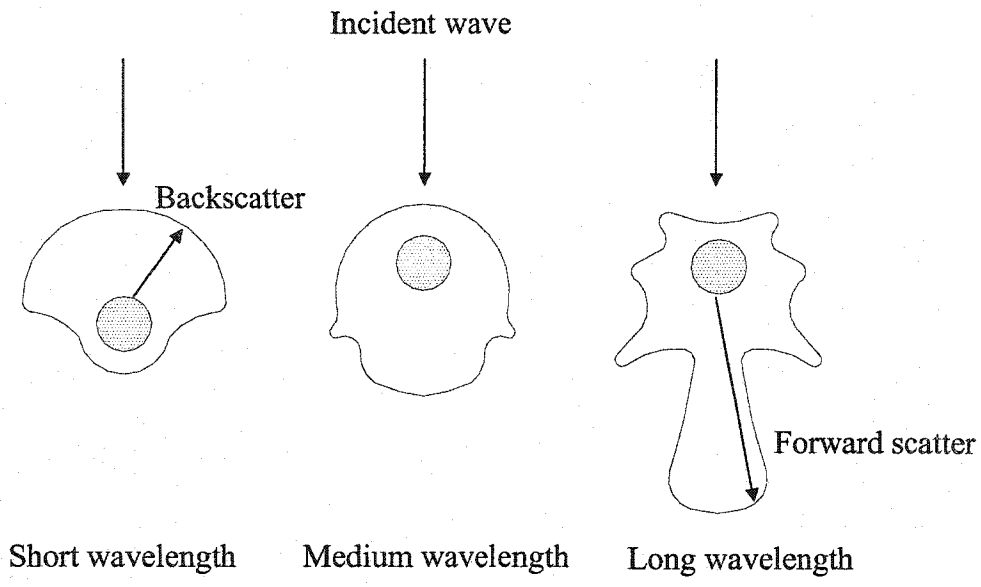

Fig. 2.4: Typical scattering patterns for a sphere [56].

2.2 Data Acquisition System

The advent of the digital age led to a change from hardware to software for all aspects of ultrasonic measurement, such as data acquisition, data processing, and display techniques. The significant development of electronics made it possible to acquire complex signals and to record and process them in short time duration. This section presents a data acquisition system for the particle detection and introduces the software used in this study.

2.2.1 Electrical Hardware Specifications

Figure 2.5 shows a block diagram of the data acquisition system hardware. It includes a digitizer CompuScope 12100 board (Gage Applied Science Inc., Montreal, Canada) with 12 bits A/D resolution and 8 Mega-bytes memory. The sampling rate is up to 100 MHz for the one-channel mode and up to 50 MHz for the two-channel mode. Two pulser/receivers (Model 5072, Panametrics Inc. or Model PR35, JSR Ultrasonics Inc.) were used to generate UTs, and each of them can be operated at different configurations with reflection and transmission. To filter out the DC components before the signals are fed to the digitizer one high pass filter is used. In addition, a frequency generator, model DG535 (Stanford Research System Inc., Sunnyvale, California, USA), is used to provide a precise repetition rate and delay to the pulser/receiver and Gage board synchronously. A 7856 oscilloscope (Tektronix) is used to monitor the signals in real time. The computer used in this study is Pentium III with a CPU of 550 MHz and 384 MB of RAM.

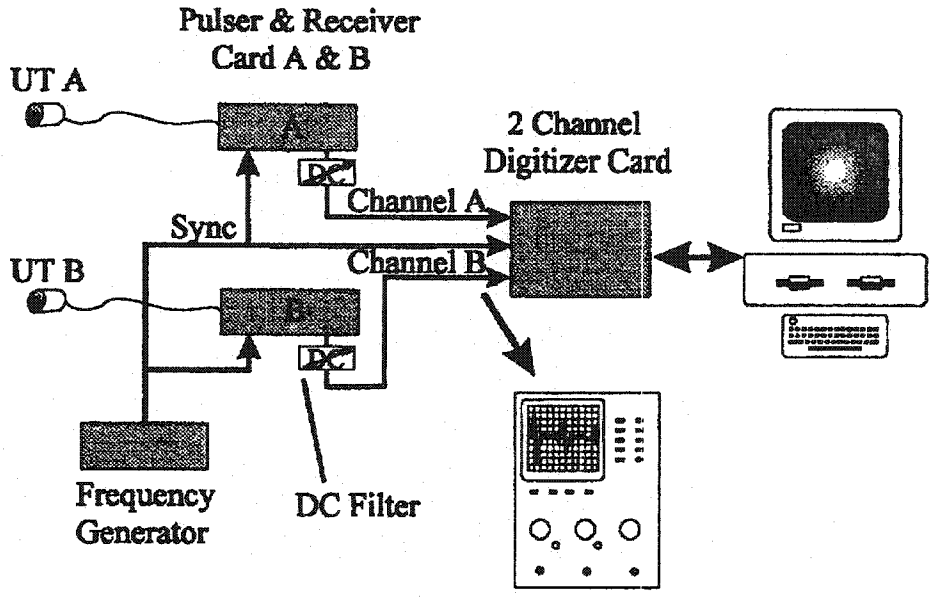

Fig. 2.5: Schematics of ultrasonic acquisition system.

2.2.2 Data Acquisition Software Application

All programs of data acquisition and processing are designed as Virtual Instruments (VIs) using Labview software (National Instruments Inc.). The VIs, are equipped with a friendly graphic interface and, therefore, allow the user to set up operation mode and data recording requests easily. In this section, the VI for data acquisition is introduced, which is primarily used in our study. Its front panel is shown in Fig. 2.6. This VI has the interface function for the selection of the trigger level, sensibility level, channel used, delay, width, etc. The data acquisition approach can be either multiple recording or serial recording. For the serial recording, the Gage board sends the signal directly to the computer. Its acquisition can be continued as long as the memory of the hard disk in the

computer is available. This advantage allows us to record all particles passing through the detection area continuously during the experiments. However, in this approach, the time for the data file to be taken and transferred depends on the computer speed. Therefore, the data transfer speed is not constant for each frame even in the same repetition rate. This means that it is difficult to analyze the movement of each particle. Fortunately, the multiple recording approach can acquire data faster than serial recording: many signals in a short period of time. The basic principle of this approach is that the recorded signals are first stored in the Gage board memory and when the memory is full the acquisition stops and the transfer from the board memory to the hard disk of the computer begins. Therefore, the speed of acquisition is constant because it depends on the repetition rates. With the help of the frequency generator mentioned above, it is possible to reach a repetition rate as high as 3000 Hz. In this case the fastest recording time is 1/3 ms for each frame. This speed is sufficient for our particle detection experiments, because the speed of 1/3 ms per frame represents that the moved distance is only 0.35 mm when the particle passes through the detection area with the velocity of 1.04 m/s (at the flow rate of 2.16 ml/s in the calibration experiments). Therefore, the multiple recording approach allows us to observe in detail the movement of each particle.

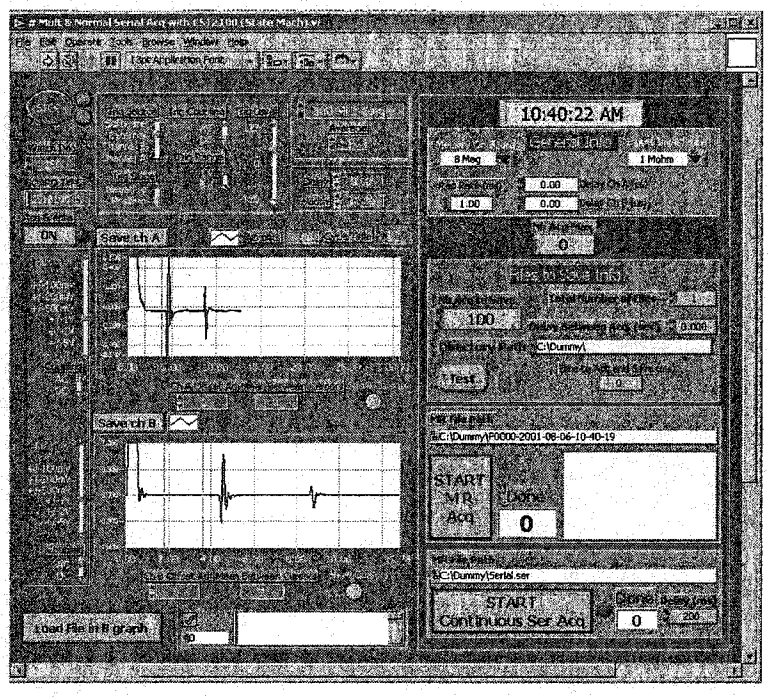

Fig. 2.6: Front panel of the VI performing data acquisition.

2.3 Summary

In order to help readers to understand this thesis, some concepts and theories that are available in many other resources, such as SNR, the reflection and transmission coefficients, ultrasound attenuation, and scattering signals were introduced in this chapter. The pitch-catch ultrasonic measurement configuration can effectively avoid spurious echoes overlapping the desired echo (L^1) during particle detection.

The data acquisition system is composed of hardware and software. The acquisition board is GAGE CS12100 with 8 MB memory. With the help of the frequency

generator, the speed of data acquisition using multiple recording approaches can be as fast as 1/3 ms per frame at a repetition rate of 3000 Hz.

Chapter 3: Buffer Rod Probes

As mentioned in Chapter 1, an ultrasonic system of high sensitivity for metal cleanliness evaluation mainly depends on the ultrasonic performance of buffer rods such as signal strength, SNR and radiation pattern. Therefore choosing a suitable buffer rod for ultrasonic measurement is crucial. The research and development of buffer rods has evolved over the last several years. The difficulty of using a long buffer rod is, in most cases, caused by spurious echoes due to dispersion, multipaths, mode conversion and beam spread in the rod with finite diameters or specific shapes. In addition, scattering echoes from random grains or voids in the rod materials are also sources of the noise that reduces the performance of the buffer rods. Our focus in this chapter is on the experimental investigation of the ultrasonic performance of buffer rods having different core materials, cladding and no cladding, and different shapes. This investigation is divided into two parts: the signal strength and SNR of the signal reflected from the probing end of the buffer rod and, the ultrasonic field distribution when the ultrasonic signals exit from the probing end and enter into the liquid (water).

3.1 Buffer Rods Configuration

It is understood that the two important parameters for evaluation of buffer rod are signal strength and SNR of the signal reflected from the probing end of the buffer rod. When one consider attenuation and reflection of ultrasound during the propagation in the buffer rod and in liquid, only a part of ultrasonic energy is transmitted into the liquid by a

transmitter probe. Furthermore, only a part of transmitted energy scattered from the particles in the liquid is received by the receiver probe in our water simulation experiments described in Chapter 4. Therefore, the signal strength is crucial for particle detection. The attenuation of ultrasound in the media depends on the microstructure of the material, ultrasonic frequency, buffer rod length and etc. (refer to equation 2-3). In our experiments here, the pulse-echo mode was used. An important parameter regarding SNR is that it is defined as the strength of the desired signals reflected echoes at the probing end over that of the unwanted echoes in the buffer rod. One way to improve SNR of a buffer rod is to reduce unwanted signals especially the trailing echoes. The trailing echoes are mainly caused by the wave diffraction and mode conversion in a rod of finite diameter and specific shape. A time interval δT, between the echo L^1 and the adjacent trailing echo can be approximately represented by the following equation [54]:

$$\delta \mathbf{T} \cong d\sqrt{\frac{1}{V_S^2} - \frac{1}{V_L^2}} \tag{3-1}$$

where d is the rod diameter, and V_S and V_L are the shear and longitudinal wave velocities respectively in the rod. We note that δT is proportional to d. When the diameter of rod increases, the time interval δT will increase as well.

The various metallic rods used are shown in Figure 3-1. Group (a) are commercially purchased rods of aluminum (Al) alloy, magnesium (Mg), titanium (Ti) and mild steel. Each has a length of 127 mm and a diameter of 25 mm and the dimensions were chosen so as to be suitable for our application. Both ends of the rods are polished and parallel to each other. Group (b) shows Al rods having a length of 152

mm with circular (ϕ19.05mm), square (16.89mm×16.89mm) and rectangular (22.45mm×12.70mm) cross section shaped but still with the same area of 285 mm^2. Group (c) shows the same Al rods as Group (b), but with stainless steel (SS) cladding fabricated by the thermal spray technique on the side of the rods [40]. The thickness of claddings is 1 to 2 mm.

Figures 3.2 (a) and (b) shows the longitudinal wave UTs used in the experiments: a), with a circular shape (Nominal frequency: 10MHz, element size: Ø9.5mm, Panametrics Inc.) and b), with a square shape (10MHz, 8.5mm×8.5mm, Japan Probe Inc., Japan). Each UT, however, had the same piezoelectric active area of 72 mm^2. These UTs were separately attached to the UT end of the circular, square and rectangular shaped rods and the ultrasonic echoes from probing end of these rods were evaluated. Different shapes of UTs and rods induced different diffraction mechanisms inside the rods and produced a different SNR.

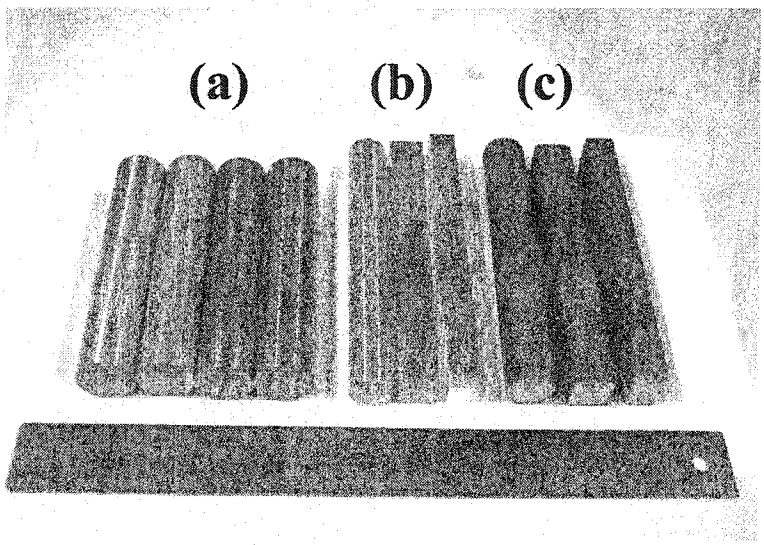

Fig. 3.1: Metallic buffer rods used for the evaluation of their ultrasonic performance.

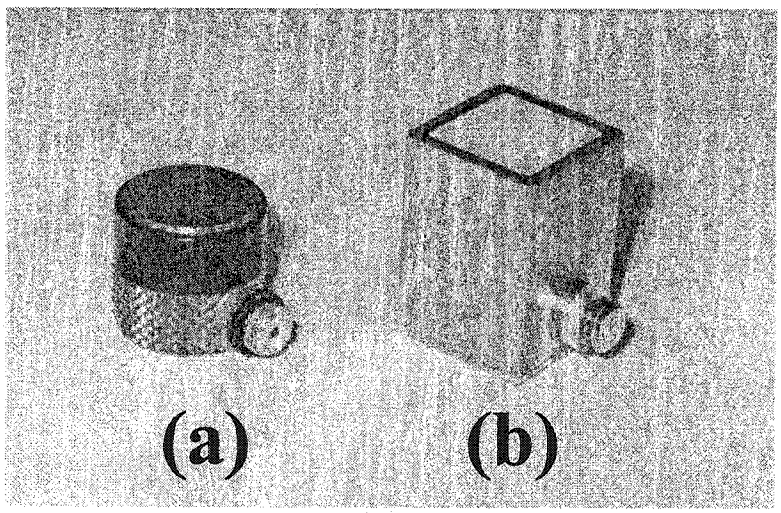

Fig. 3.2: Longitudinal wave ultrasonic transducers with shapes of circle (a) and square (b).

3.2 Buffer Rod Evaluation

3.2.1 Rod Material

Ultrasonic propagation in different materials have differing velocities. In order to investigate the effects of material properties on the signal strength and SNR of rods, four kinds of metal rods are chosen as shown in Fig. 3.1 (a). The measured velocities in these four rods are given in Table 3-1.

Table 3-1: Velocities of longitudinal, V_L, and shear, V_S, waves for four metallic materials [59].

Material	V_L (m/s)	V_S (m/s)
Mild Steel	5960	3235
Al	6374	3111
Mg	5823	2930
Ti	6130	3182

It is understood that enlarging the diameter d of a rod can reduce the amount of mode conversion at the periphery of the buffer rod and thus reduces the trailing echoes. Increasing the d means that SNR is also enhanced. Furthermore, as indicated in Eqn. (3-1), d is enlarged, δT increases. The calculated δT 's for the four metals given in Table 3-1 are shown in Fig.3.3 as a function of the diameter d from 0 to 80 mm.

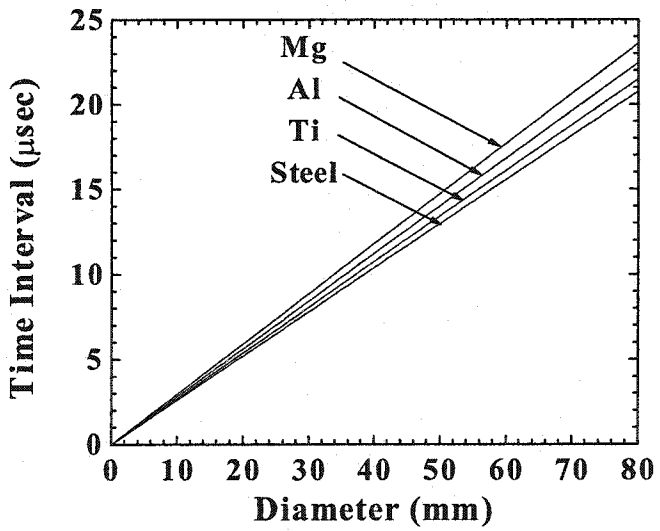

Fig. 3.3: Calculated δT's for Mg, Al, Ti and steel rods as a function of the rod diameter d.

This figure is helpful for designing a buffer rod. For example, it can predict that the first trailing echo would appear 6.49 μs after the main echo L^1 for the mild steel rod having a diameter of 25 mm.

The ultrasonic measurement results for the four rods shown in Fig. 3.1 (a) using a circular UT of 10 MHz and 9.5 mm diameter illustrated in Fig. 3.2 (a) are presented in Fig. 3.4. It is seen for each metallic rod that trailing echoes appear with a constant time interval δT after L^1. The time delay t_{dL1} ($t_{dL1} = 2l/V_L$) of L^1 in each rod depends on the longitudinal wave velocity, V_L and the length of l.

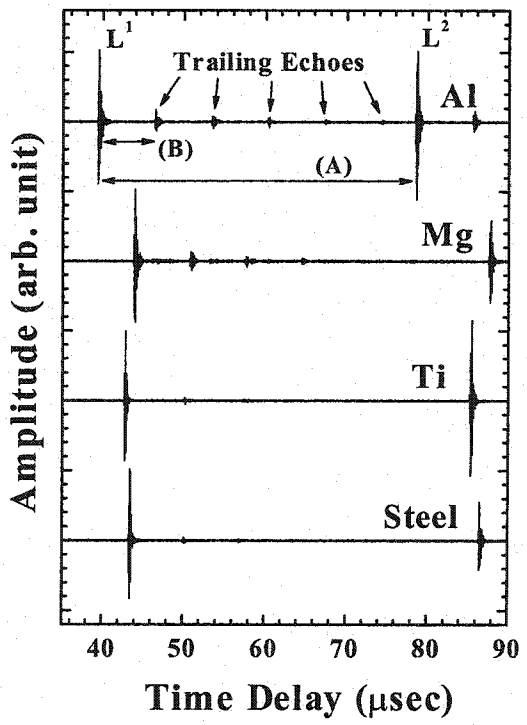

Fig. 3.4: Measured ultrasonic signals between L^1 and L^2 in the four rods described in Table 3-1.

The signal strength (amplitude) and the SNR of L^1 obtained for each rod shown in Fig. 3.4 are presented in Table 3-2. In Table 3-2 the signal strength of each rod has been normalized by that of the mild steel rod. The SNR is calculated as the amplitude of L^1 over that of the largest spurious echo appearing in the following two time delay ranges; namely (A) between L^1 and L^2 and (B) between L^1 and the 1^{st} trailing echo as shown in Fig. 3.4.

One can see that the 1^{st} trailing echo is the largest spurious echo in the range of (A). The SNRs of the signals, L^1, in mild steel and Ti rods are 27 dB and 26 dB, respectively. They are about 10 dB better than those in Al and Mg rods in the range of (A) as shown in Table 3-2. In addition, the signal strength of L^1 in the steel rod is the largest and 6 dB better than that of the Ti rod. It is considered that the signal strength of L^1 depends on ultrasonic coupling (acoustic impedance matching) between the UT and the rod at the UT end as well as the elastic properties and microstructures of the rod material. The rod material causes ultrasonic attenuation due to the wave diffraction, scattering and absorption in the rod.

The L^1 signals in Al, Ti and mild steel rods have almost the same SNR of 38 dB in the range of (B) where the scattering echoes from the random grain in the rod would be dominant as the spurious echoes. Under the present experimental conditions it can be concluded that the L^1 signal in the mild steel rod has the strongest signal (largest amplitude) and the best SNR among four purchased rods.

Table 3-2 Signal strength and SNR of L^1 for the time delay range (A) between L^1 and L^2 and (B) between L^1 and the 1st trailing echoes with different rod materials.

Material	Signal strength (dB)	Signal-to-noise ratio (dB)	
		(A)	(B)
Al	-12	16	37
Mg	-18	17	29
Ti	-6	26	38
Steel	0	27	38

3.2.2 Rod Shape

In order to investigate the effects of shapes of the buffer rods on the signal strength and SNR, Al rods were prepared as shown in Fig. 3.1 (b). The Al and shapes are chosen based on better ultrasonic coupling with water and economical concerns. The signal strength and SNR of L^1 in the Al rods of three different shapes are evaluated using 10 MHz UTs that have a circular or a square shape as shown in Fig. 3.2. The measurement results of the ultrasonic echoes reflected from the probing end of the Al rods with three different shapes using circular UT of 10 MHz and 9.5 mm diameter are shown in Fig. 3.5. One can see that the trailing echoes appear for the square and rectangular rods as well as for the circular rod. In the case of the square UT of 10 MHz and 8.5 mm × 8.5 mm, the trailing echoes are also observed for all the rods but the amplitude is smaller than the case of the circular UT for each rod. Table 3-3 shows that the signal strength of L^1 for each combination of the rods and the UTs are normalized by the one obtained for the square rod using the circular UT. It is found that the signal strength of L^1 obtained from the

square UT is smaller than that obtained from the circular UT for each rod. In addition, the signal strength of L^1 in the circular rod is 7 to 15 dB smaller when compared with that in the square and rectangular rods for each UT. It is believed that these are not only due to the performance of the UT itself but also due to the difference of the wave diffraction in rods of different cross-section shapes with UTs having different shapes. Further investigation will be conducted in the future.

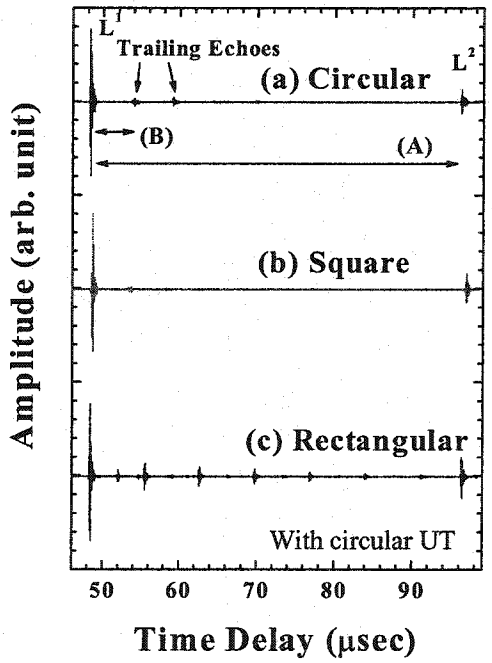

Fig. 3.5: Measured ultrasonic signals between L^1 and L^2 in the three Al rods as shown in Fig. 3.1 (b) having the cross-section of (a) circular (b) square and (c) rectangular, but with the same cross-section area of $285mm^2$.

Table 3-3: Signal strength of L^1 in the Al rods with three different cross-section shapes and two different UT's of circular and square shapes.

Rod shape	**Signal strength (dB)**	
	Circle UT	**Square UT**
Circle	-15	-17
Square	0	-8
Rectangle	-2	-10

Table 3-4: SNR of L^1 in the Al rods with three different cross-section shapes and two different UT's of circular and square shapes for the time delay duration (A) and (B) shown in Fig. 3.5.

Rod shape	**Signal-to-noise ratio (dB)**			
	(A)		**(B)**	
	Circle UT	Square UT	Circle UT	Square UT
Circle	21	36	37	40
Square	28	34	44	41
Rectangle	14	23	43	45

Table 3-4 shows the SNR of L^1 in the Al rods with three different cross-section shapes and two different UT's of circular and square shapes for the time delay duration (A) and (B) shown in Fig. 3.5. In the case of the circular UT, the L^1 in the square rod has the best SNR of 28 dB in the range of (A). The overall best SNR of 36 dB is achieved

with a combination of the circular rod and the square UT in the range of (A). This is probably due to the less symmetrical geometry with respect to the rod axial direction. In the range of (B), although the SNR of L^1 in the circular rod with the circular UT is 37 dB, the other combinations achieve more than 40 dB. It should be noted that the same experiments were performed using rods having the same length of 152 mm as the presented rods but having a cross-section area of 506 mm^2, which is 1.8 times larger than the presented one. The same tendency of the signal strength and the SNR of L^1 given in Tables 3-3 and 3-4 related to different rod cross-sections and different shapes of UTs were observed.

3.2.3 Cladding

Reports state that cladding can enhance the SNR and improve the ultrasonic guidance in the buffer rods [40,44]. Therefore, in this continuing study, the stainless steel (SS) claddings were fabricated, by the thermal spray technique as shown in Fig. 3.1 (c), on the side of Al rods having the same dimensions as the ones presented in the previous section 3.2.2. The ultrasonic echoes reflected from probing end were measured by the circular and square UTs as described in section 3.2.2. Figure 3.6 shows the measurement results obtained from the circular UT and evidences the finding that the trailing echoes are significantly diminished due to the cladding. The same results were obtained using the square UT. The reason for this decrease in trailing echoes is that thermal sprayed claddings have high porosity which leads to high ultrasonic loss. The high porosity

greatly reduces the wave reflection and mode conversion at the core/cladding boundary [41].

Table 3-5 shows the strength of L^1 signals for Al rods having three different cross-section shapes obtained from the signals shown in Fig. 3.6. It is noted that the signal strength is normalized by that of the non-clad square Al rod with the circular UT as shown in Fig. 3.5 (b) in order to compare with non-clad rods. Reports state that the cladding could enhance the wave guidance resulting in larger signal strength compared to non-clad rods [40,44]. In our experiments the signal strength for the circular cladding rods with the circular UT is 8 dB greater than that for non-clad ones. However, the variations of signal strength when comparing clad with non-clad rods were only within ± 2dB for the other combinations of the rods and UTs. This means that the cladding does not increase the signal strength of L^1. The detailed explanation will be investigated in another study. The amplitude of L^1 could be affected by the different surface conditions such as flatness and roughness at the interface between the UT and rod surface at the UT end. Table 3-5 presents the SNR of L^1 for the cladding rods shown in Fig. 3.1(c) in the time delay range of (A) as indicated in Fig. 3.6. The SNR of more than 40 dB is achieved in L^1 signal for all the combinations of the buffer rods and the UTs presented in Table 3-4 due to the SS cladding.

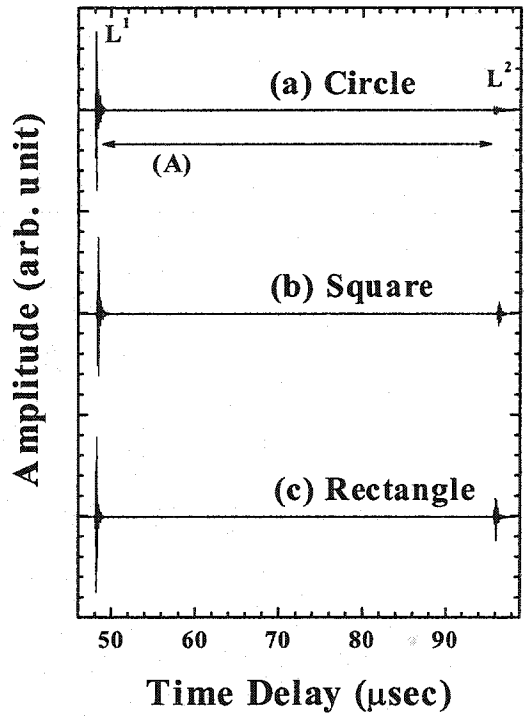

Fig. 3.6: Measured ultrasonic signals between L1 and L2 in the SS cladding Al rods of three different cross-section shapes using a circular UT of 10 MHz and 9.8 mm diameter.

Table 3-5: Signal strength of L^1 in the SS cladding Al rods with three different cross-section shapes and two different UT's of circular and square shapes.

Rod shape	**Signal strength (dB)**	
	Circular UT	**Square UT**
Circle	-7	-18
Square	1	-8
Rectangle	-4	-8

Table 3-6: SNR of L^1 in the SS cladding Al rods with three different cross-section shapes and two different UT's of circular and square shapes for the time delay duration (A) shown in Fig. 3.6.

Rod shape	SNR (dB)	
	Circular UT	Square UT
Circle	40	41
Square	41	41
Rectangle	42	41

3.3 Ultrasonic Field Distribution (UFD)

For developing a water simulation system to detect particles, knowledge about field distribution of the ultrasonic wave exiting from the probing end of the buffer rod and entering into the water is important, since the strength and shape of ultrasonic beams determine the ultrasonic sensing area in liquid. In addition, it is necessary to know the area, where the strength of the ultrasound is assumed to be uniform, for sizing particles using the amplitude of scattered ultrasound. Several techniques for predicting the ultrasonic field distribution measured by single UT have already been reported [60-64]. In our study, we apply the technique based on a small ball bearing immersed in water as an ultrasonic target in the pitch-catch mode. The reason for applying the pitch-catch mode instead of the pulse-echo mode is that it can provide improved SNR. This technique is used because (1) it is a simple measurement procedure for determining the spatial ultrasonic field quantities in water; (2) the measurement conditions are similar to

that for particle detection in water; (3) it provides good spatial and temporal resolutions; and (4) two scan directions (X-Y and axial X-Z) can be facilitated easily for a spatial field evaluation, as long as an axial-symmetry UFD can be assumed [65-66].

Fig. 3.7 is a schematic of the setup of our ultrasonic field distribution experiments. A 3.2 mm diameter stainless steel ball bearing as the reflector was placed in a tank filled with degassed water. A 5 MHz longitudinal UT with 3 mm piezoelectric active element diameter was placed in the tank as ultrasonic receiver and was located as high as the top of the ball bearing as shown in Fig. 3.7. The reason for choosing such frequency UT is that we only have 5 MHz UT which can be immersed in the water as a receiver. The distance between the surface of UT receiver and the center of the ball bearing was 34.0 mm. The value of this distance was made as short as possible in order to achieve a high signal strength while avoiding the rod touching the receiver during scanning. Another UT designated as the transmitter was placed at the UT end of the buffer rod. This probe was fixed on the micro-precision positioning system for our scanning system and controlled by a PC computer through a IEEE GPIB board. The computer was programmed via Labview to acquire and process ultrasonic signals. The A/D board was a CS12100 card with 12-bit resolution and 8 Mega-bytes memory. The UTs were driven by a PR35 pulser/receiver in the transmission mode where signals were received at 100 MHz sampling rate.

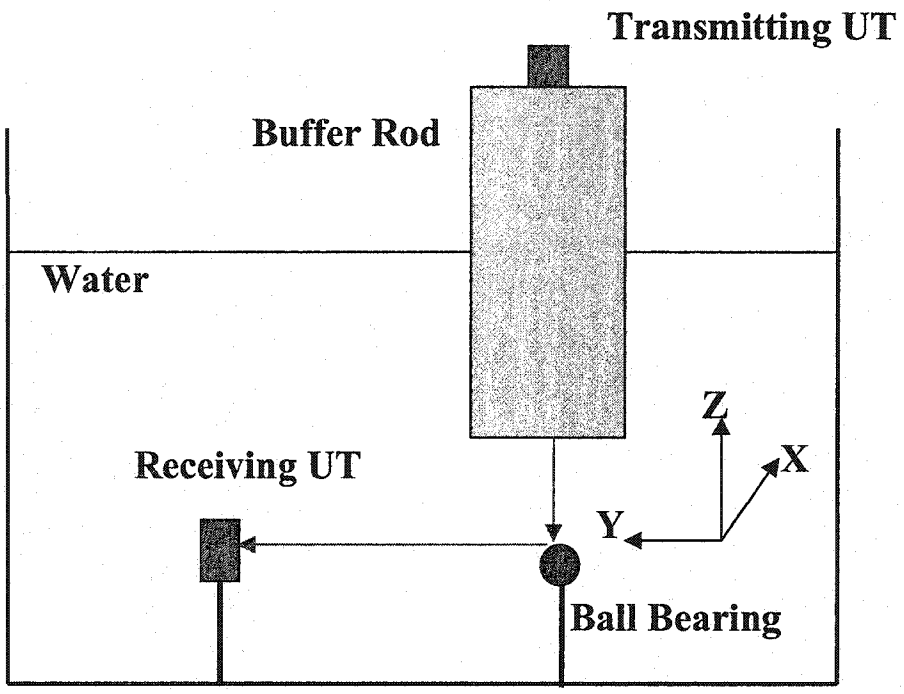

Fig. 3.7: Schematic of the setup of ultrasonic field distribution experiment.

In order to investigate the effects of the shapes of the UFD patterns, cross-section shapes such as circle, square and rectangle cladding Al rods with the same length of 152 mm as shown in Fig. 3.1 (c) were chosen. The scanning operating with a 10 MHz circular longitudinal UT of 9.5 mm diameter as the transmitting UT was carried out in X-Y plane defining as X-Y scan. The scan area was 30 mm × 30 mm, the grid scan-step size space was 0.2 mm for both directions.

Figures 3.8, 3.9 and 3.10 show the scanned images of the UFD with the distance of 10 mm between the end of rod and the top of the ball bearing for cladding Al rods with square, circle and rectangle shapes respectively. In these figures the white lines are the

real size and shape of buffer rods, and each separated contour line is 3 dB apart of signal amplitude. As expected, the results clearly indicated the shape of ultrasonic wave patterns depended on the shape of the buffer rods instead of the shape of the UT. Furthermore, it should be noted that the rod length of 152 mm is larger than the *Fresnel* distance, $d^2/4\lambda$ = 46.6 mm, where d is a diameter of the UT and λ is a longitudinal wavelength in Al [67]. Therefore, it is our conclusion that the ultrasonic radiated in water from the probing end is in the far-field region (*Fraunhofer* Zone).

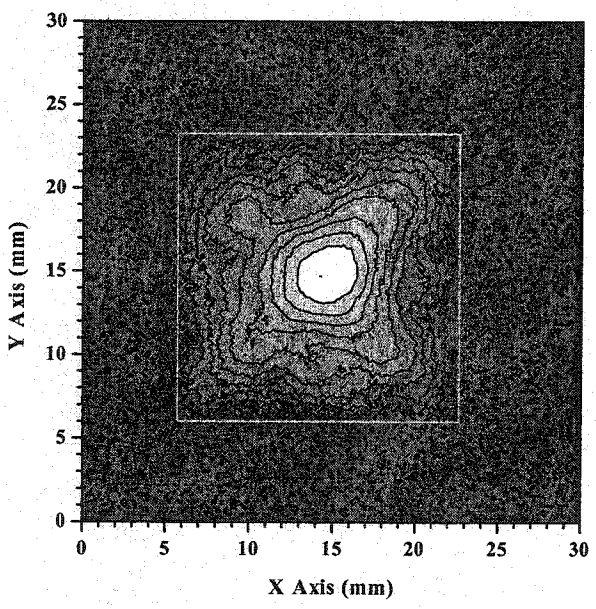

Fig. 3.8: Scan image of the UFD with the distance of 10 mm between the end of rod and the top of ball bearing for cladding Al rods having square cross-section shape of 16.89 mm×16.89 mm using a circular UT of 10 MHz and 9.8 mm diameter.

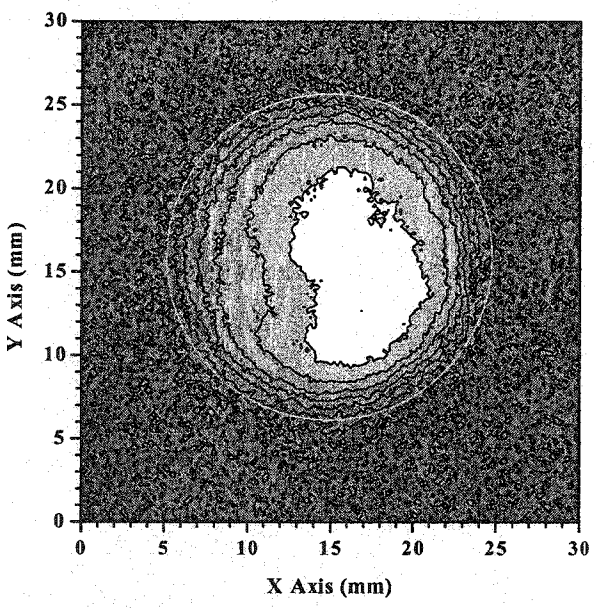

Fig. 3.9: Scan image of the UFD with the distance of 10 mm between the end of rod and the top of ball bearing for cladding Al rods having circle cross-section shape of 19.05 mm diameter using a circular UT of 10 MHz and 9.8 mm diameter.

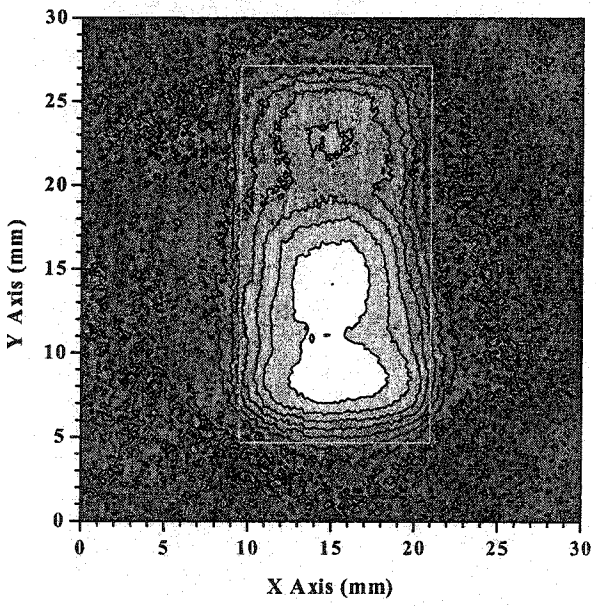

Fig. 3.10: Scan image of the UFD with the distance of 10 mm between the end of rod and the top of ball bearing for cladding Al rods having rectangle cross-section shape of 22.45 mm×12.70 mm using a circular UT of 10 MHz and 9.8 mm diameter.

Comparing the images shown in Figures 3.8, 3.9 and 3.10, we found that the strong signal areas were different in the UFD of the buffer rod with different shapes, even though the same measured distance was used. By plotting the signal amplitude along the X direction for square and circle rods with 1 mm, 10 mm and 30 mm distance as shown in Fig. 3.11 (a) and (b) respectively, it is clearly indicated that the strong signal area of the circular rod is larger than that of the square rod. The widths at -6 dB line of the circular and square cladding Al rods at distances of 1mm, 10 mm and 30 mm were measured (see Fig. 3.11) and the results were shown in Table 3-7. These results mean that the circular shaped rods produced more uniform ultrasonic beam in water than the square rod.

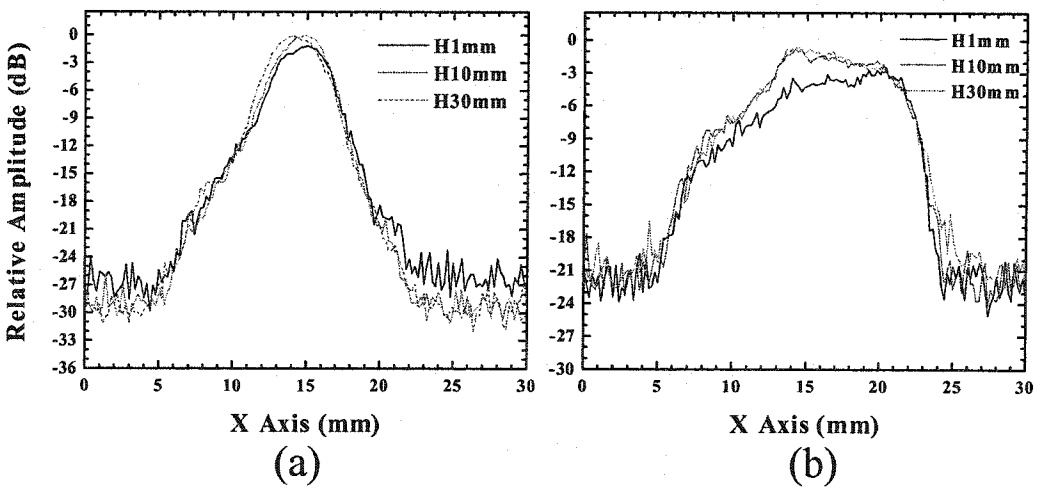

Fig. 3.11: Signal amplitude of UFD for square (a) and circle (b) cladding Al rods presented in Figs.3.1 (c) with the distance of 1 mm, 10 mm and 30 mm using a circular UT of 10 MHz and 9.8 mm diameter.

Table 3-7: Measured UFD beam widths at -6 dB line of circular and square cladding Al rod at distances of 1mm, 10mm, and 30mm, as shown in Fig. 3.11.

Distance (mm)	-6dB width (mm)	
	Square	Circle
1	4.54	9.28
10	5.00	10.98
30	5.26	11.02

Four other scanning experiments were performed with the same alignment as above and 5 MHz receiving the circular UT of 3 mm diameter as described before. In the first experiment, in order to determine the effect of the shape of the transmitting UT, we performed the same UFD experimental setup used in Fig. 3.8 except that the transmitting UT was a 10 MHz square similar to the one shown in Fig.3.2 (b) rather than the circular one in a). Fig. 3.12 shows the scanned image of the UFD for cladding Al rods having square cross-section shape of 16.89 mm × 16.89 mm using a 10 MHz square UT of 8.5 mm × 8.5 mm element at the distance of 10 mm. There is no observable difference between the results presented in Fig.3.12 and Fig.3.8. In the second experiment, in order to determine the effect of the frequency of transmitting UT, we used a 5 MHz circular UT of 9.8 mm diameter as transmitting UT instead of the 10 MHz UT used in Fig. 3.8. The UFD result is given in Fig. 3.13. By comparing Fig.3.13 and Fig.3.8, it is observed that the 5 MHz UT produces a cleaner image than the 10 MHz UT. The main reason is that the center frequencies of the UTs for the transmitter and the receiver are the same. Also

another reason is that there is less attenuation with a lower frequency in water. In the third experiment, in order to determine the effect of an area of cladding on the buffer rod, we also performed the UFD for a square shaped cladding buffer rod (CBR) of 22.50 mm × 22.50 mm. Fig. 3.14 shows the UFD result of this large area CBR using the 10 MHz circular UT shown in Fig. 3.2 as the transmitting UT at the distance of 10 mm. By comparing Fig.3.14 and Fig.3.8, it is observed that large area CBR has a larger sensing area than the small area CBR. Note that the image in Fig. 3.14 is not symmetrical. The possible reasons would be: (1) the end of the buffer rod is not polished uniformly; and (2) the elastic properties of the buffer rod are not axially symmetric. In the fourth experiment, in order to determine the effect of the length of the cladding buffer rod, we performed the same UFD experimental setup used in Fig. 3.8 except that the length of CBR was 101.3 mm long rather than that of 152 mm long. Fig. 3.15 shows the UFD result of this short CBR using the 10 MHz circular UT shown in Fig. 3.2 as the transmitting UT at the distance of 10 mm. By comparing Fig.3.15 and Fig.3.8, it is observed that short CBR has a cleaner and larger sensing area than the long one. This is reasonable because there is less ultrasonic attenuation in the buffer rod.

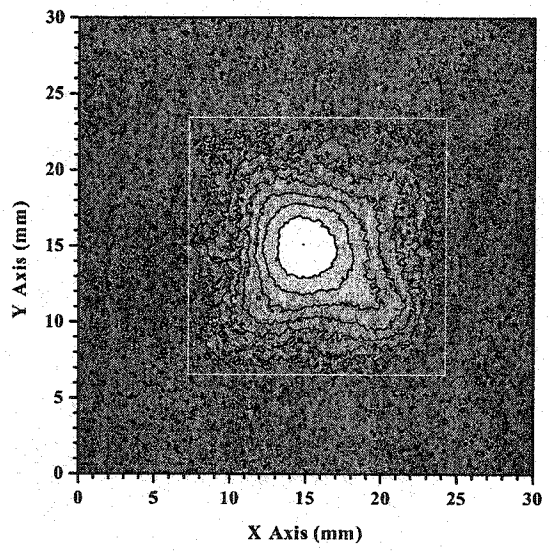

Fig. 3.12: Scan image of the UFD for cladding Al rods having square cross-section shape of 16.89 mm×16.89 mm using a 10 MHz square UT of 8.5 mm × 8.5 mm element at a distance of 10 mm.

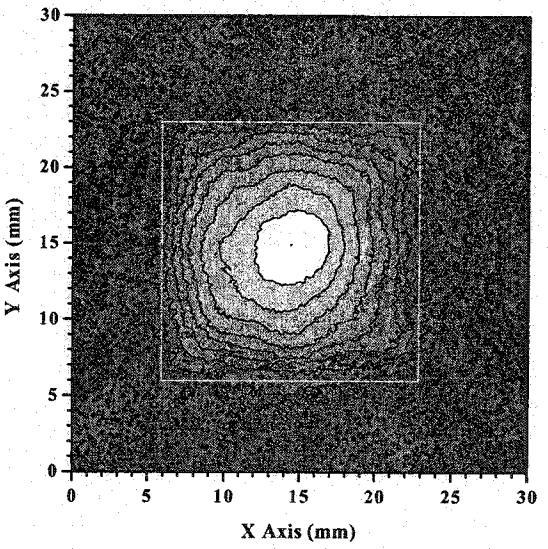

Fig. 3.13: Scan image of the UFD for cladding Al rods having square cross-section shape of 16.89 mm×16.89 mm using a 5 MHz circular UT of 9.8 mm diameter at a distance of 10 mm.

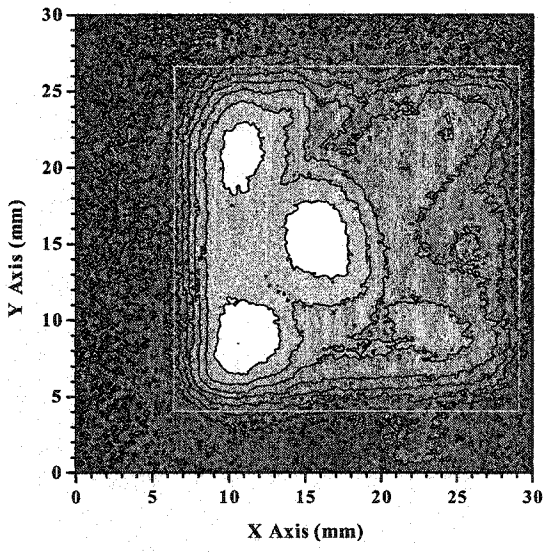

Fig. 3.14: Scan image of the UFD for cladding Al rods having square cross-section shape of 22.50mm×22.50mm using a 10 MHz circular UT of 9.8 mm diameter at a distance of 10 mm.

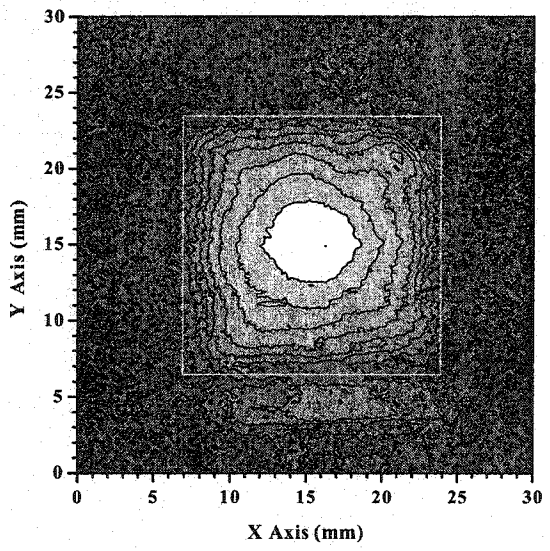

Fig. 3.15: Scan image of the UFD for cladding Al rods having square cross-section shape of 16.89 mm×16.89 mm and 101.3 mm long using a 10 MHz circular UT of 9.8 mm diameter at a distance of 10 mm.

Finally, in order to investigate the changes of UFD with the changes in the distance, X-Z plane scan experiments were carried out. Two examples are shown in here. The first example illustrates the experimental setup for Fig. 3.8 where an X-Z scan was carried out instead of an X-Y scan. The second one illustrates an X-Z scan for the experimental setup for Fig. 3.14. In these two experiments, the scanning distance is from 1 mm to 30 mm along Z direction. The scanning step in X direction remains constant at 0.2 mm while Z direction changes to 0.5 mm. The UFD is shown in Fig. 3.16 and Fig. 3.17 respectively. These images show that the UFD maintains a relatively uniform strength when the distance away from the probing end of the CBR is between 10 mm to 30 mm. Therefore, this distance can be applied to ultrasound paths between the probing end and the detected particles.

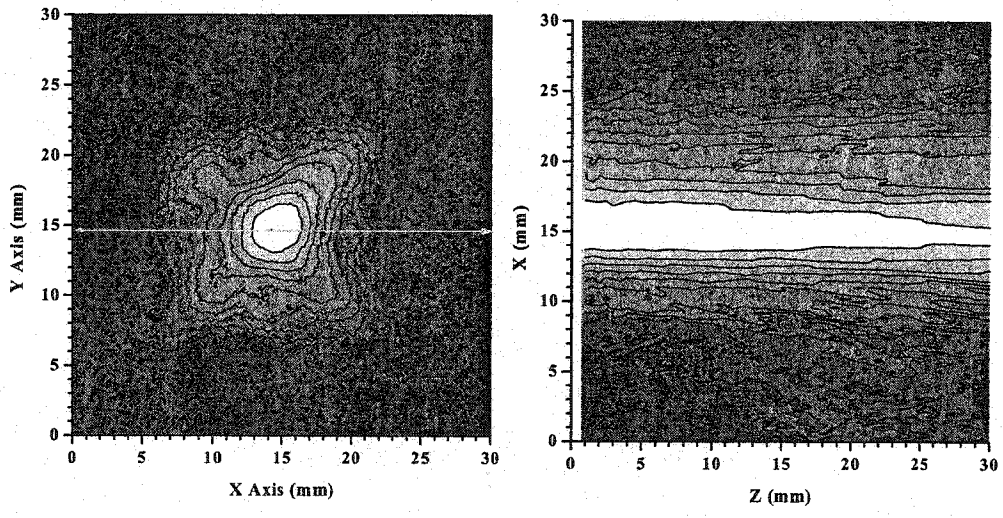

Fig. 3.16: Scan image of the UFD for cladding Al rods having square cross-section shape of 16.89 mm×16.89 mm using a 10 MHz circular UT of 9.8 mm diameter: the left one is for X-Y scan; the right one is for X-Z scan.

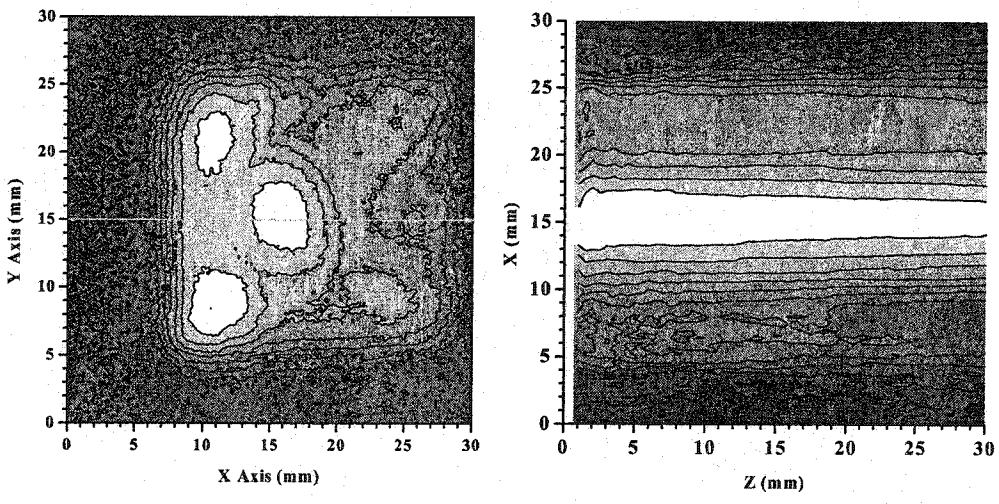

Fig. 3.17: Scan image of the UFD for cladding Al rods having square cross-section shape of 22.50 mm×22.50 mm using a 10 MHz circular UT of 9.8 mm diameter: the left one is for X-Y scan; the right one is for X-Z scan.

3.4 Summary

In order to obtain high ultrasonic performance results in signal strength and SNR, this chapter has focused on studying the effects of rod materials, rod cross-section shapes and cladding. First, the rod materials were investigated using purchased rods made of Al alloy, Ti, Mg, and mild steel and it was found that the mild steel rod carries the strongest signal and the highest SNR of 27 dB in signal L^1 reflected from the probing end of the buffer rod. Next, the effects the shapes of the rods had on the SNR were investigated using Al rods having three different cross-section shapes using UTs of both a circular and a square shape. In the case of the circular UT, the square rod produced the highest SNR of 28 dB in signal L^1. The highest SNR of the three, with an SNR of 36 dB in signal L^1 was achieved with a combination of the circular rod and the square UT. This is due to a less symmetrical geometry with respect to the rod axial direction. As well, the SNR of more than 40 dB in L^1 was achieved for all the combinations of the rods and the UTs by fabricating the SS cladding.

UFD experiments demonstrated that ultrasound radiated in water from the probing end is in the far-field region and the shape of the ultrasound beam is the same as the shape of the rod. Since the beam width is associated with the particle detection area, our results showed that the circular rods have a larger beam width. It was also observed that the 5 MHz UT offered larger sensing area in water than the 10 MHz UT mainly due to less attenuation in water. In Figs. 3.16 and 3.17 the axial UFD showed that the beam

width remained relatively uniform for Z = 10 mm to 30 mm and, therefore, this range should be chosen for particle detection.

Chapter 4: Water Simulation System

On-line methods to evaluate the cleanliness of molten metals by counting the number and measuring the size of inclusions are highly desired in metal manufacturing industries. In this chapter we will establish the procedure, to investigate the experimental possible configurations and to evaluate the sensitivity, accuracy, inspection volume and speed for cleanliness evaluation of molten metals using ultrasound for a particle flow simulation system using water. This water simulation system plays an important role in the development of the method and system for ultrasonic evaluation of molten metal cleanliness. The water simulation system has advantages as follows: (a) the experiments can be carried out at room temperature, and therefore, they are safe; (b) the experimental situations can be observed in action by allowing the interface conditions between the probing end and the water visible. Such direct observation provides greater reliability, reproducibility and confidence with the experiment; (c) it can reduce the cost for design and optimization of the system for molten metals.

4.1 The Principle and Methods

As illustrated in Chapter 1 a buffer rod can be used as a probe to perform ultrasonic measurements in molten metals at elevated temperatures. Therefore, buffer rods are used in the study of this chapter and they will be employed in molten metals. Fig. 4.1 shows the ultrasonic method for counting the number and measuring the size of particles in

liquids with a pitch-catch configuration. A pair of ultrasonic probes each of which is a buffer rod are installed in the liquid tank. The basic principle of ultrasonic detection is that one probe (indicated as "Transmitter") transmits the ultrasonic plane waves into liquid and another one (indicated as "Receiver") receives the signals scattered by the particles passing through the sensing area This scattered signal carries information about ultrasonic properties such as velocity, attenuation, number, size, and shape of the inclusions in the liquid. The variation of the velocity, attenuation and the scattered energy of the ultrasound propagating in liquid can be used to characterize the inclusions. The amplitude of this scattered ultrasonic signal may be used to measure the particle size and each detection provides a count for the particle. It should be noted that a pulse-echo configuration is also available. In this configuration, any one of the two probes shown in Fig. 4.1 can serve as both the transmitter and the receiver. The reason for choosing the pitch-catch mode is that this configuration can provide a scattered signal of high SNR.

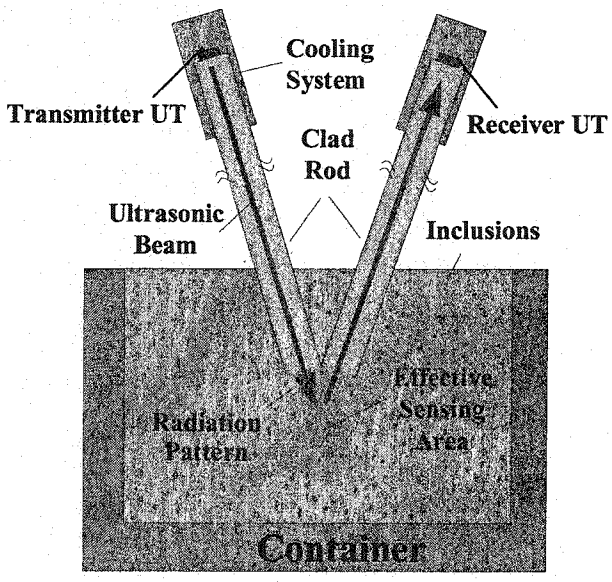

Fig. 4.1: Ultrasonic method for counting the number and measuring the size of particles in liquids with a pitch-catch configuration.

To detect the minimum size of the particles, the SNR of the desired signal does not solely depend on the frequency (wavelength) of the ultrasound but also on the signal strength. More ultrasound energy is required in order to detect small sized particles. In principle, a low frequency ultrasound reduces the ultrasonic attenuation and a high frequency provides a short wavelength which affords high resolution. In our lab UTs of 1 MHz to10 MHz are available [44-46]. In this study, optimal selection of the operating ultrasonic frequency is required. 5 MHz and 10 MHz UTs were chosen because these frequencies are proper for buffer rod size used in the experiments and the ultrasonic pulse width (time resolution) is suitable for detecting particles in our experimental conditions.

When buffer rod probes are inserted into a liquid, the ultrasonic reflection and transmission coefficient can be calculated by Equations 2-1 and 2-2. In this thesis, aluminum (Z_1 = 17.33×10^6 kg/m^2-s) [59] was employed as buffer rod material in water (Z_2 = 1.491×10^6 kg/m^2-s) [68]. Then using Eqn. 2.2, T = 0.16. This means that 16% of ultrasonic amplitude (strength) was transmitted into water, 84% was reflected back to the probe at the interface. If we choose steel (Z_1 = 47.1×10^6 kg/m^2-s) [59] buffer rods to detect particles in molten magnesium (Z_2 = 10.12×10^6 kg/m^2-s) [69], the transmission coefficient T=0.36. The study indicates that the transmitted ultrasonic strength in molten Mg will be higher than in water. The attenuation of ultrasonic power propagating in the liquid can be calculated by Eqn. 2-3. The attenuation constants (α) for water and molten Mg at 725 ^{0}C are 25.6 [68] and 1.2 (10^{-15}s^2/m) [69] at 10 MHz frequency, respectively. Since the attenuation in water is greater than that in molten Mg, an ultrasonic signal of

sufficient strength can be obtained in molten Mg. Therefore, our water simulation system has worse condition than the applications in molten metals.

Figure 4.2 shows a schematic of an ultrasonic probe installed in the water simulation system. The probe consists of an Al rod with a square cross-sectional area of 17 mm × 17 mm and a length of 152 mm. The square shape was chosen due to the larger signal strength and higher SNR compared to that of the circular and rectangular shapes [70]. A square sleeve, having the same length of the Al rod, made of a thin brass plate or plastic plate is attached to the four sides of the Al rod with an air gap of 1mm. This air gap prevents the leakage of ultrasound from the side faces of the Al rods into water and vise versa. The sleeve is an important element since such leakage causes the crosstalk between the transmitter and receiver probes in the pitch-catch mode. This crosstalk will induce the spurious noise so as to reduce the SNR of the desired signals scattered from the particles. For the molten metal applications, we can use clad steel buffer rod, or steel or stainless steel as a sleeve material in molten Mg. Two ultrasonic probes having the same dimensions as shown in Fig. 4.2 in pitch-catch configuration are used for the experiments.

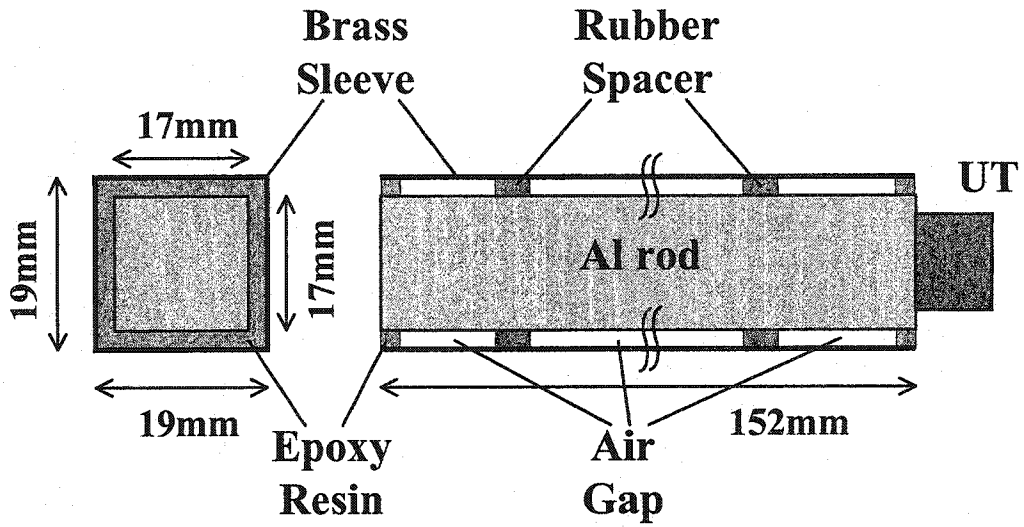

Fig. 4.2: Schematic of an ultrasonic probe installed in the water simulation system.

In the water simulation system, polyvinyl chloride (PVC) particles are used as inclusions in molten metals. There are three factors to consider when employing PVC inclusions. One is that PVC particles can be easily separated (dispersed) in water, and therefore, ensuring ultrasonic scattering echo from a single particle is a key point in this study. The second is that the density of PVC equals 1.36 g/cm^3,which is a little heavier than water, for this reason PVC particles can be suspended in water through the stirring process. The third is that the ratio of the acoustic impedance of PVC over that of water is close to that of the acoustic impedance of the magnesium oxide (MgO) over that of molten Mg. In other words the scattered signal strength from PVC in water is similar to that from MgO in molten Mg.

In attempting to detect small sized particles, increasing the SNR effectively (reducing the noise level) is crucial. There are two noise sources in addition to those in buffer rods and the electric noise induced from the electronic instruments: impurities and

air bubbles inside water. In order to prevent foreign particles and air bubbles in water from affecting the measurement, all water used was carefully prepared by filtering and degassing. We used a vacuum pump and/or boiling to achieve degassing.

4.2 Water Simulation System

Figure 4.3 shows a block diagram of one particle flow simulation system using water. The system is composed of two water tanks, a water pump, a flow meter, tubes, and a mixer. The tubes, having different inner diameters, are made of glasses, polymers or metals such as stainless steel, aluminum and copper, etc, are used to guide the particles and ensure that the particles pass through the detection area. The water containing the particles, whose size and number were to be evaluated, was stored in the tank (left). In order to distribute the particles uniformly in water, the water in the tank (left) was stirred by a mixer (Magnetic Stirrer: Model 84, Cole & Parmer, Germany) for the duration of the particle injection into the ultrasonic sensing area in the water tank (right). An appropriate amount of water was filled into the tank (right) before the injection. The flow rate of the water was controlled by the water pump and obtained by measuring the flowed water volume per unit time or by a flow meter. This system was equipped with a pair of Al buffer rods (mentioned before) with transducers, pulser/receiver and a PC computer with acquisition board. The ultrasonic signals are recorded and stored by the personal computer with an A/D converter with a resolution of 12 bits and a sampling rate of 100MHz. Sampling rate directly affects the accuracy of measurement. In our water simulation experiments, the pulsed ultrasonic frequency is 5 MHz or 10 MHz, which

means their Nyquist frequency is 10 MHz or 20 MHz. Our sampling rate is 10 or 5 times larger that the Nyquist frequency. Therefore, the sampling rate of 100MHz is sufficient for particle detection in our experimental conditions.

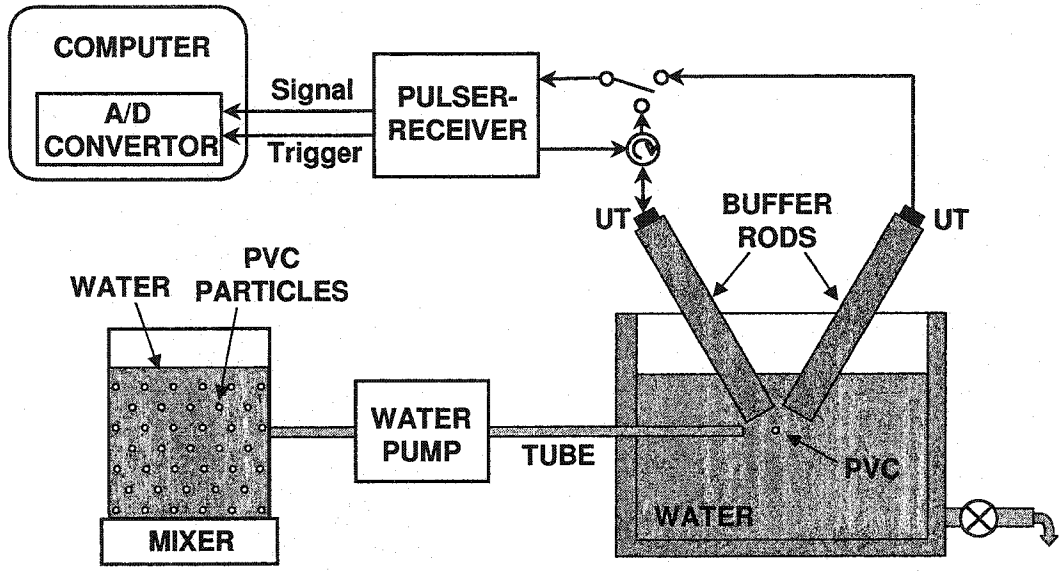

Fig. 4.3: Block diagram of particle flow simulation system using water.

4.3 Experiments and Results

4.3.1 Particle Concentration Measurement

We will illustrate the evaluation of the PVC particle concentration in water in this section. During molten metal processing, inclusion concentration is one of the important

parameters for quality assessment. Figs. 4.4 and 4.5 show pictures of the ultrasonic system for particle concentration measurement. A pair of Al rods (shown in Fig. 4.2) tilted with a 90° separation and a 4.4mm distance between the tops of rod ends were immersed into the water. In the future, different angles will be examined to have best sensitivity. At the UT ends of rod UTs were attached through an ultrasonic couplant (Sonotech, Inc.). In this experiment, 10 MHz circular UTs (Model A127S, Panametrics Inc.) and a puler-receiver (Model PR35, JSR Ultrasonics Inc.) were used. The pulser/receiver was set at Energy = 1, PRF = 0.5 kHz and Gain = 79 dB (maximum value) in this case. The signals were recorded through serials recording approach, which allowed for an extended length of time for data acquisition, as mentioned in Chapter 2.

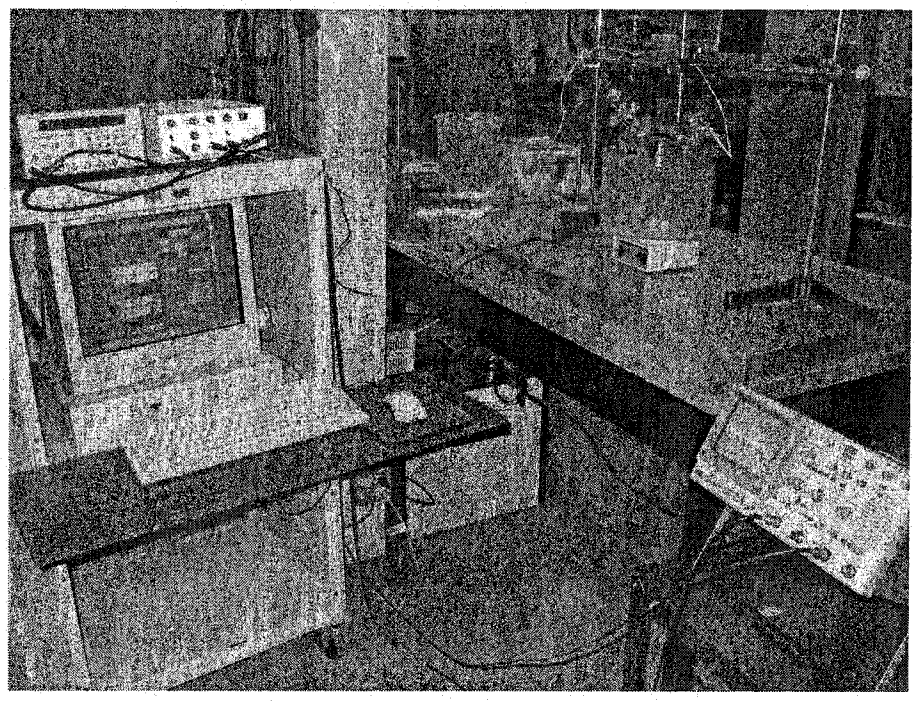

Fig. 4.4: Photo of ultrasonic system for particle concentration measurement.

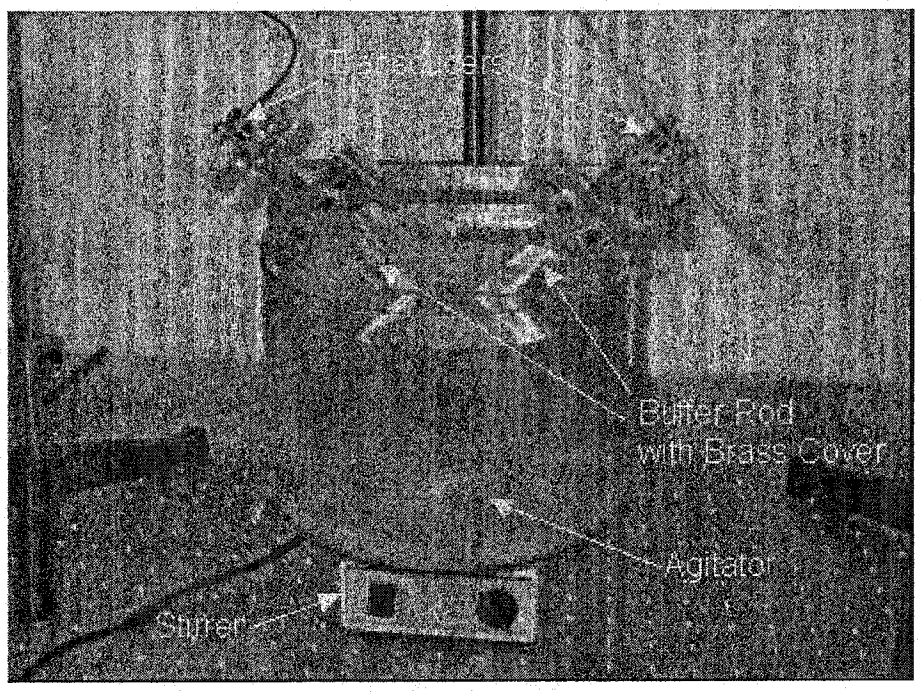

Fig. 4.5: Ultrasonic probes immersed in the water tank filled with PVC particles.

PVC particles as inclusions were added to the water to form different volume concentrations of 10 ppm, 25 ppm, 50 ppm, 75 ppm and 100 ppm. Fig. 4.6 shows two images of PVC particles with mean diameters of 30 μm and 125μm supplied by Goodfellow Cambridge Limited. During the experiment, continuous stirring by a magnetic stirrer ensured uniform particle distribution in water.

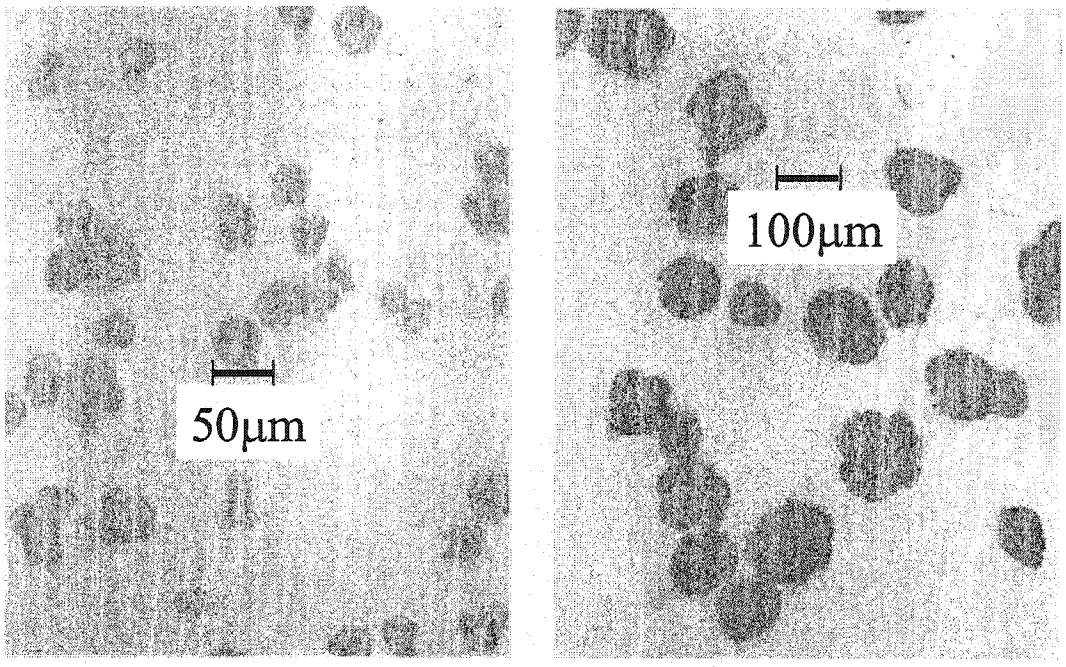

Fig. 4.6: Two images of PVC particles with mean diameters of 30 μm (left) and 125 μm (right) supplied by Goodfellow Cambridge Limited.

Figure 4.8 shows an example of the measurement results of different particle volume concentration of 100 ppm, 50 ppm, 10 ppm and 0 ppm respectively. The horizontal axis is the time delay and indicates how long it takes when ultrasound propagates from the transmitting UT to the receiving UT. The vertical axis is the measurement time where each frame interval is 4 seconds for this experiment. In this configuration (90 degrees) as shown in Fig. 4.7, the time delay of the signal reflected from the center of the detection area can be calculated by:

$$t_d = \frac{2l_B}{V_{Al}} + \frac{w_B + \sqrt{2}d_t}{V_W} \tag{4-1}$$

where, l_B and w_B are the length and width of buffer rod respectively; d_t is the distance between the tops of rod end; and V_{Al} and V_W are the ultrasonic velocities in Al rod and water, respectively. In this case:

When: l_B = 152mm; w_B = 17mm; d_t = 4.4mm;

V_{Al} = 6374 m/s [59]; V_W = 1491 m/s [68]. $\Rightarrow$ t_d = 63.3 μs.

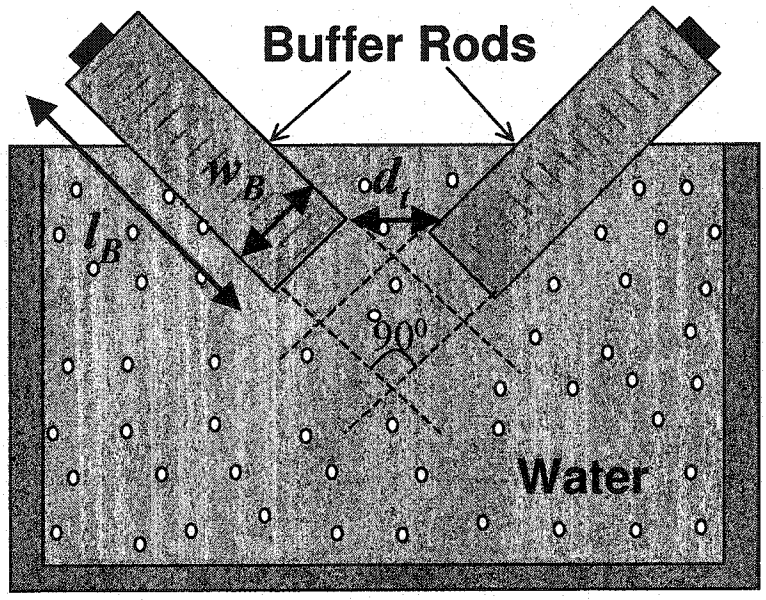

Fig. 4.7: Schematic diagram of 90 degrees configuration of pitch-catch mode.

The experimental results also show that the signals appear at the 64 μs location within the time domain, which confirms that these signals come from the particles when they pass through the detection sensing area. (Referring to the graphs in Fig. 4.8) From the graphs, one can see that for pure water (0 ppm) the graph is clean, and as the particle concentration increases, more signals appear. This result proved that our ultrasonic system could distinguish the particle concentration.

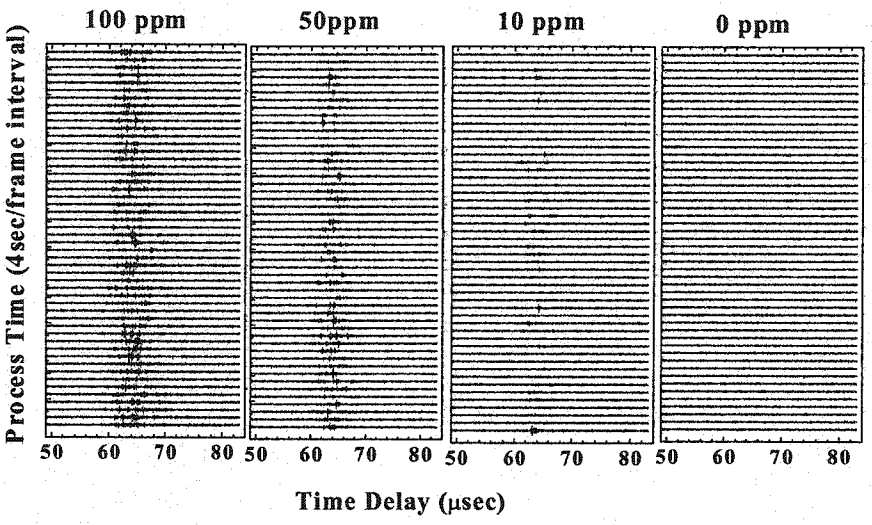

Fig. 4.8: The signals obtained for different PVC particle concentrations: 100 ppm, 50 ppm, 10 ppm and 0 ppm in water.

By taking the envelop of the signal amplitude and calculating the average amplitude for each data, the averaged amplitude was plotted for 100 ppm, 75 ppm, 50 ppm, 25 ppm, 10 ppm and 0 ppm are shown in Fig. 4.9 as snap shuts at different times. As we can see, high concentration increased the possibility of particles appearing in the detection area. By plotting the peak value of the average amplitude for each concentration and size of particles, the relationship between average amplitude, concentration, and size of particles was obtained as shown in Fig. 4.10. These figures demonstrate the linear relationship between the average amplitude of ultrasonic signals and particle concentration. As we expected, measured results also showed that a large average amplitude of signal was reflected by a large sized particle. Therefore, there could be a relationship between the amplitude of scattered signal and the particle size.

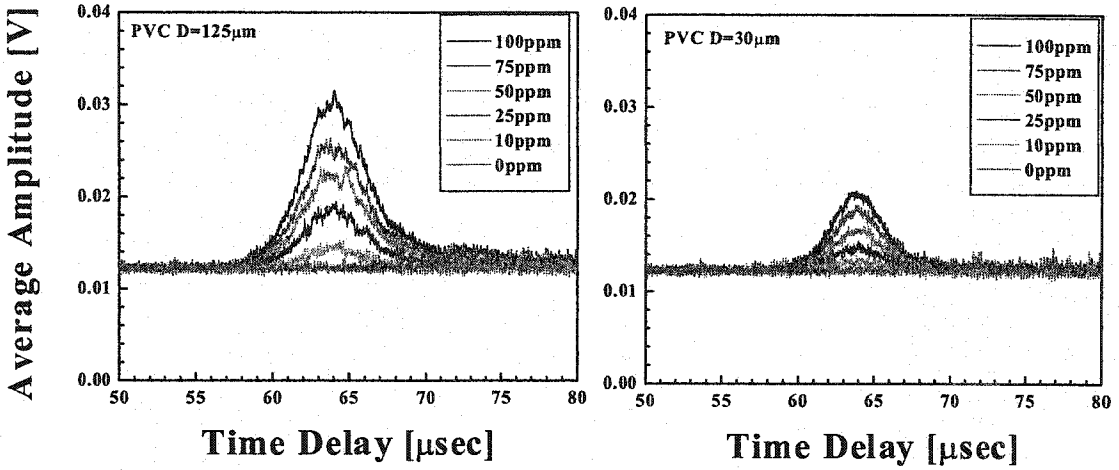

Fig. 4.9: Averaged amplitude plots for 100 ppm, 75 ppm, 50 ppm, 25 ppm, 10 ppm and 0 ppm as snap shuts at different times: the left is for the particle having mean diameter of 125 μm and the right is that of 30 μm.

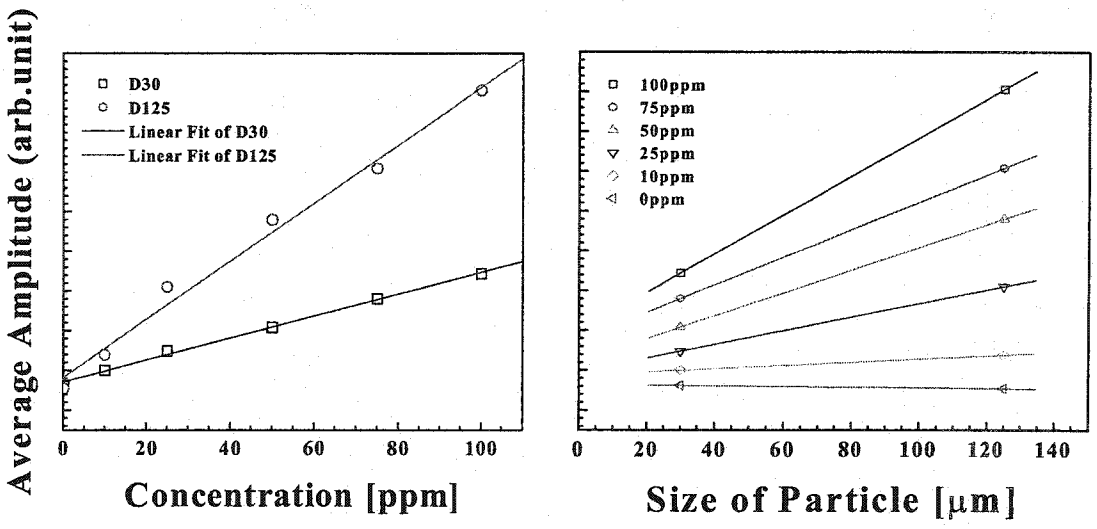

Fig. 4.10: Relationship between average amplitude and concentration, size of PVC particles.

4.3.2 Counting the Number of Particles

For manufacturing involving molten metals, accurate information regarding the number of inclusions in molten metals is highly desired. In this section, the technique for counting of the PVC particles in water is developed.

In the experiments, the ultrasonic probes' setup (angle and distance) was the same as shown in Fig. 4.5, and the method was described in section 4.2. The key in our approach is to use a tube to guide particles so as to ensure that they are injected into the sensing area in the water one by one. Two configurations of particle injections were investigated as shown in Figs. 4.11 (a) and (b), the particles are injected into the water horizontally and vertically, respectively in (a) and (b). It was assumed that the path of the particle movements is straight and passes into the center of the sensing area as shown in Fig. 4.11. In the case of (a), since the time delays of the signals reflected from particles anywhere on the path in the sensing area are nearly the same, only one particle must be present in the sensing area in order to obtain the signal reflected from a single particle. In the case of (b), the time delays of the signals reflected from the particles at different positions on the path are not the same, hence, signals scattered from more than one particle could be obtained separately in the time domain. Therefore, because multiple particles could be present in the sensing area at the same time for the configuration in (b) but not in (a), the configuration of (b) should be used rather than that of (a) when the number of inclusions present in the sensing region is more than one.

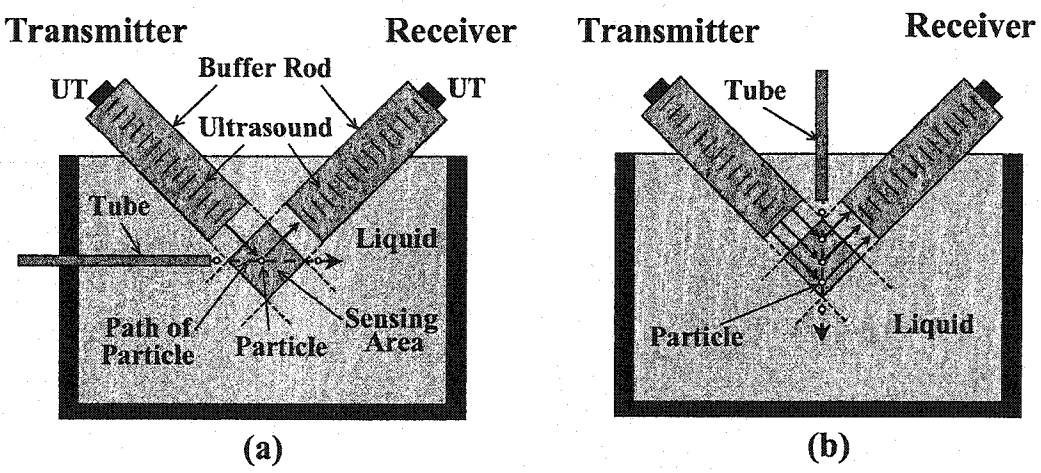

Fig. 4.11: Concepts of particle detection in liquids using ultrasonic pitch-catch configuration. The particles are injected horizontally (a) or vertically (b) through the tube.

Figure 4.12 shows the experimental setup. Water with PVC volume concentrations, C, of 5 ppm or 10 ppm was prepared in a bottle, separately. Fig. 4.13 shows the size distribution provided by the commercial source of the PVC particles used where a mean diameter, d_{mp}, of the particles was 125 μm, and the flow rate, Q, of the water transferred from the tank (A) to the tank (B) through the tube by air pressure was 2.16 ml/sec. It should be noted that the flow rate is related to the inspection volume. Large inspection volume is desirable. A stainless steel tube with an inner diameter of 1.62 mm was used since the sizes of the inclusions in molten Al or Mg which are of our interest are, in general, less than 1mm.

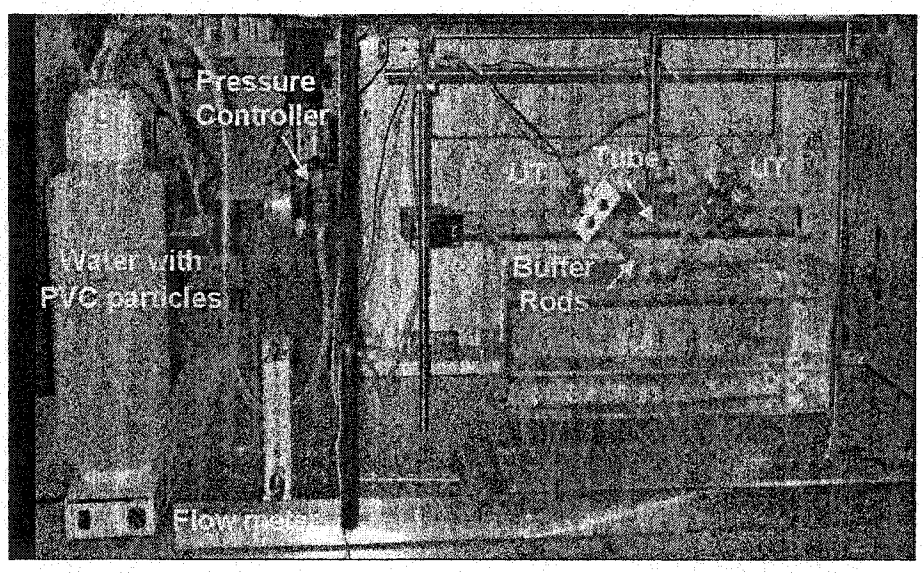

Fig. 4.12: Photo of experimental setup for counting the number of PVC particles in water.

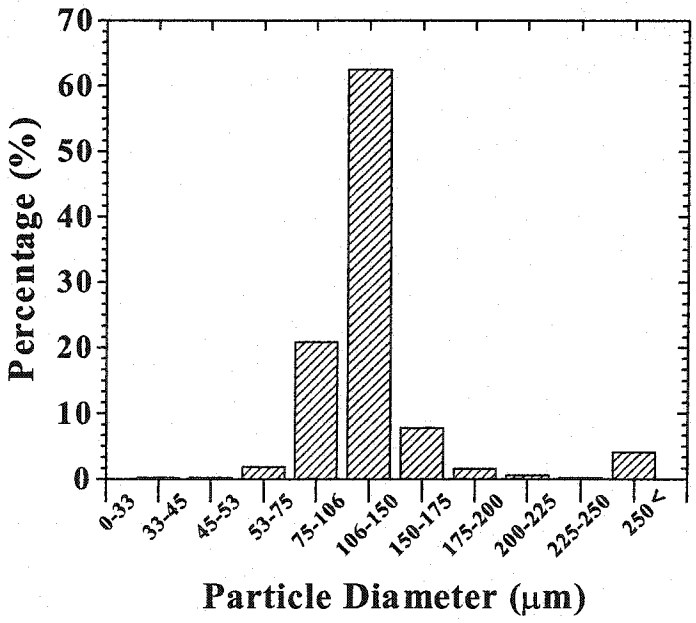

Fig. 4.13: Size distribution provided by the commercial source of the PVC particles used in the experiments.

In this experiment, a pulser/receiver (Model 5072PR, Panametrics Inc.) was used, and it was set as Energy = 4, PRF = 1.0 kHz and Gain = 50 dB. In addition, a digital delay/pulse generator (Model DG535, Stanford Research Systems Inc.) was used because it provides a precise repetition rate and delay. A Tektronix 7856 oscilloscope was employed to observe and monitor the signals in real time, because when the acquisition of multiple recording starts, the signal monitor on VI program is frozen due to the fastest acquisition and the signals cannot be seen in the VI monitor on computer screen.

Here, the multiple recording data acquisition technique was applied because it can acquire data at the frame rate of 1 msec. Generally, each of our data file consisted of 2000 frames, and for each experiment, we acquired at least 50 files.

First, we performed the experiment without PVC particle in order to determine the spurious signals and noise level, which enables us to distinguish the desired signals, scattered from particles in the sensing area, from the undesired signals.

Figures 4.13 (a) and (b) show the typical signals obtained with horizontal and vertical injection configurations, respectively. The signals were recorded every 1 msec using the multiple recording approach with a time window of 20 μsec. In the case of horizontal injection as shown in Fig. 4-13 (a), the signals reflected from one PVC particle appeared at a constant time delay of ~64 μsec. This suggests that the particle moved straight trajectory as shown in Fig. 4.11 (a). The signals scattered from the particle were observed for 10 msec.

In the case of vertical injection, as shown in Fig. 4.14 (b), the time delay of the signals scattered from the particles increased linearly during the process time with the largest signal obtained at a time delay of ~64 μsec. This also means that the particle moved in a straight trajectory as shown in the Fig. 4.11 (b) with a constant speed. From the signals shown in Fig. 4.14 (b) with vertical injection configuration, the moving speed of the particle and the effective sensing area could be calculated, which will be discussed later. Thus, it can be concluded that the vertical injection configuration is better than the horizontal injection configuration. Furthermore, these results also verified that the particle movement in the ultrasonic sensing area was controlled by the air pressure and tube used in the system.

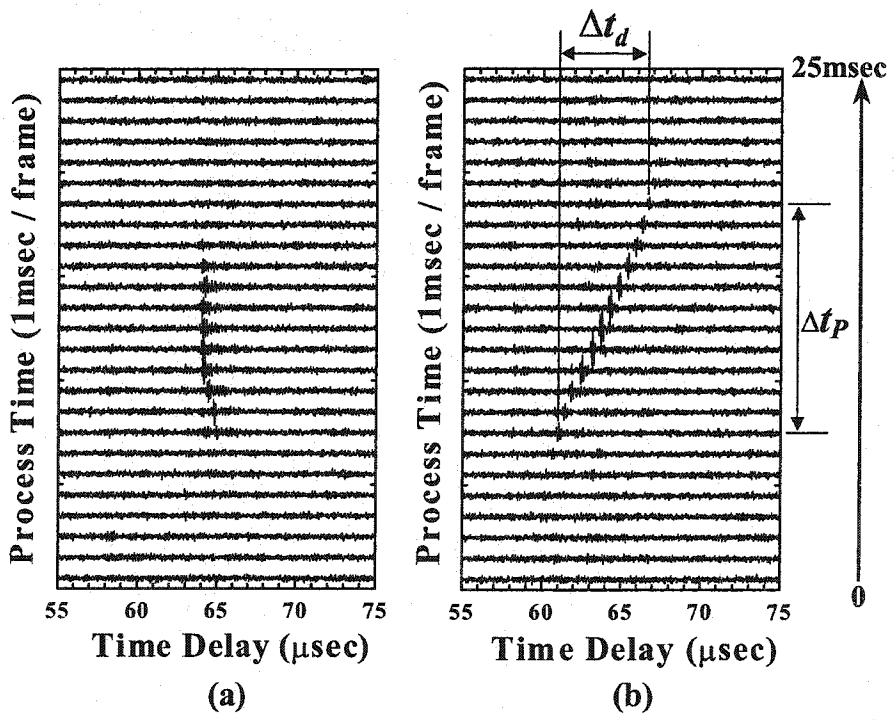

Fig. 4.14: Typical signals obtained with horizontal (a) and vertical (b) injection configurations shown in Fig.4.10 (a) and (b), respectively, at 10 MHz.

The maximum value of amplitude of the signal for each frame is plotted with respect to the process time. Figures 4.14 (a), (b) and (c) show the results for the PVC concentrations of 0 ppm, 5 ppm, and 10 ppm with the horizontal injection configuration for the process time, t_p, of 2 sec. In the case of 0 ppm, water without PVC particles flowed and signals were recorded with the same conditions as in the cases of 5 ppm and 10 ppm. The result obtained for 0 ppm shown in Fig. 4.15 (a) provides the noise level of 0.175 V, indicated by the dashed lines in Fig. 4.15, in our presented ultrasonic measurement system. When the water carrying the PVC particles passes through the detection region, one can see pulselike shapes in the curves shown in Figs. 4.14 (b) and (c). We consider that each pulse is composed of the ultrasonic signal scattered from a single particle and the peak amplitude value for each pulse is associated with the size of the particle detected. The number of the pulses having a peak value of more than the noise level (0.175 V) were counted at 20 and 41 for 5 ppm and 10 ppm of the PVC particles in water, respectively.

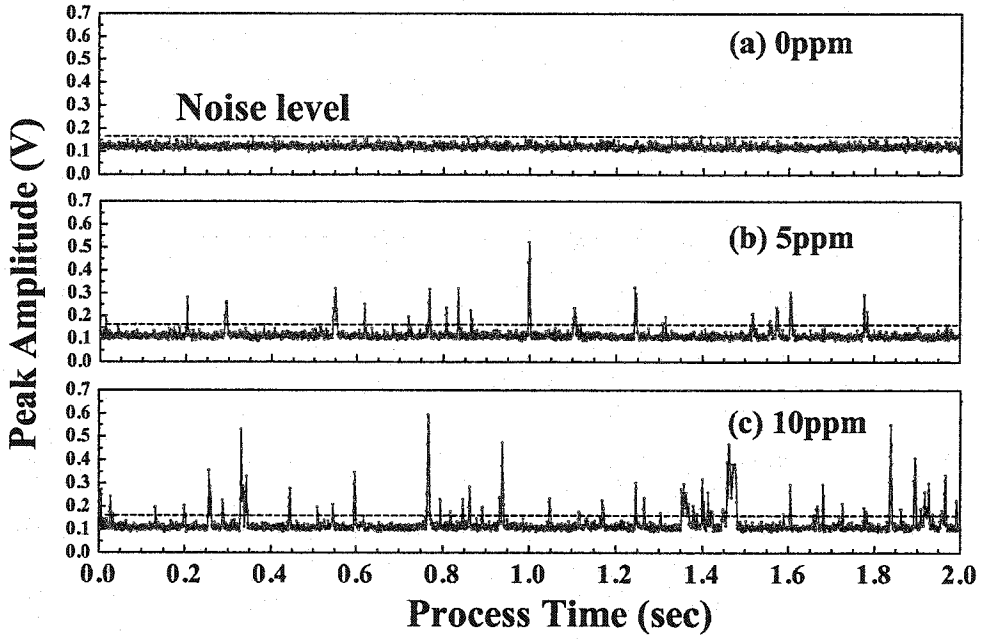

Fig. 4.15: Peak amplitude obtained from the signal for each frame shown in Fig. 4.14 (a) with horizontal injection configuration shown in Fig. 4.11 (a). The volume concentrations of the PVC particle in water were 0 ppm (a), 5 ppm (b) and 10 ppm (c). The dashed line indicates the noise level.

The number of the particles, N, passing through the sensing area for the process time, t_p, can be approximately calculated by the following equation:

$$N = \frac{6CQt_p}{\pi d_{mp}^3} . \qquad (4\text{-}2)$$

where C is the volume concentration of PVC particles in water with the values of the parameters, C, Q, t_p and d_{mp}, used in the experiments presented above, $N = 20$ and $N = 39$ for $C = 5$ ppm and $C = 10$ ppm, respectively obtained using Equation (4-2). Therefore, the experimental results presented above agreed with the calculated results. It is noted that, after many measurements for 5 ppm and 10 ppm cases, the errors of the counts

obtained by the presented method were always within 10% or two counts of the calculated results both in horizontal and vertical injection configurations.

Furthermore, we found the particle movement speed, V_f, in the sensing area was useful information for obtaining the actual measurement conditions such as flow speed and inspection volume of the liquid. For example, we can adjust the flow rate or data acquisition speed using V_f determined so as to have enough series of signals from each particle to determine the maximum amplitude for sizing the particle. The V_f could be calculated from the durations of the time delay, Δt_d, and the process time, Δt_p, as shown in Fig. 4.14 (b), where the signals from the particle appearing in vertical injection configuration. When the particles move in a straight trajectory in the sensing area, as shown in Fig. 4.11 (b), the vertical component of the particle speed, V_f, is given by:

$$V_f = \frac{V_w}{2\cos\frac{\theta}{2}} \cdot \frac{\Delta t_d}{\Delta t_p} \quad , \tag{4-3}$$

where V_w is the longitudinal wave velocity in water and θ is the angle between two probes. The V_f was calculated to be 0.54 m/s using equation (4-3), where the θ and V_w were 90° and 1491m/s at a temperature of 23°C [68], respectively, in the experiments.

From the peak values of the pulses shown in Figs. 4.14 (b) and (c), the size distribution of the PVC particles were investigated. The numbers of peak values in each range of 0.05 V were counted using the data shown in Fig. 4.15 (b) and (c) for the PVC concentrations of 5 ppm and 10 ppm, respectively. The results are presented in Fig. 4.16.

One can see that the peak amplitude distribution corresponds qualitatively well to the size distribution of the particles when compared with the data shown in Fig. 4.13. If the curve of amplitude distribution is similar with that of the size distribution, the relationship between them could be built up. It should be noted that the smallest amplitude region of 0.175 V-0.2 V in Fig. 4.16 is the half range of 0.05 V due to the noise level of 0.175 V. Therefore, the small particles, which produce signals of a the peak amplitude values of less than 0.175 V, might be missed in the counting. Detection sensitivity needs to be improved further by increasing the SNR of the system in order to detect these smaller particles.

Therefore, it was expected that the particle size and its distribution could be determined when the relationship between the amplitude and the particle size is obtained using the commercially available PVC particles having different diameters of known-size.

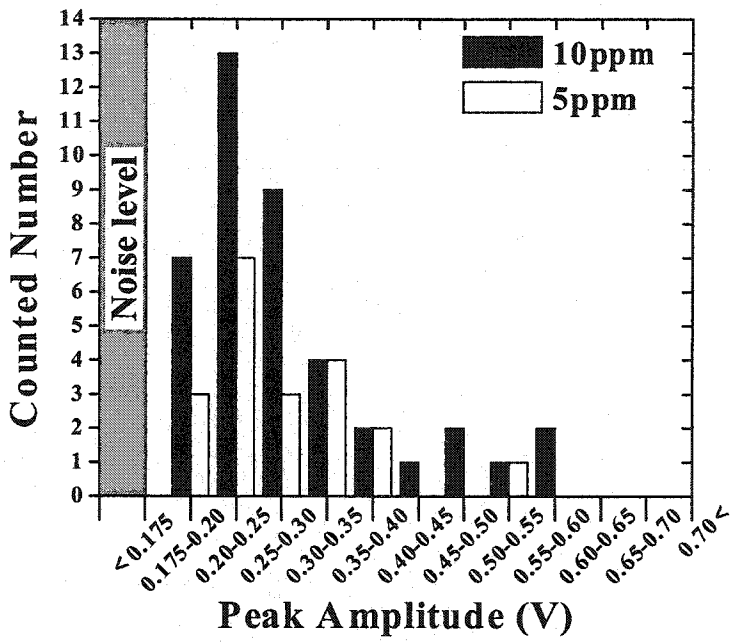

Fig. 4.16:Distributions of peak amplitude obtained from the data shown in Figs. 4.14 (b) and (c) for the PVC concentrations of 5 ppm and 10 ppm in water, respectively.

4.3.3 Measuring Size of Particles

As mentioned previously, in order to measure the size of individual particles from the amplitude of the scattering signal, the relationship between amplitude and particle size need to be known. Therefore, calibration experiments with known-size particles were carried out. The same setup as counting experiments was used except with different rods and UTs. In this experiment, the length of the rods was 101.3 mm instead of 152 mm used in the previous section. This length was two thirds of the length of the one shown in Fig. 4.2. The shorter length was chosen so that a higher strength ultrasonic signal and SNR could be obtained to detect the size of the smaller particles. Two square 5 MHz UTs (8.5 mm × 8.5 mm, Japan Probe Inc., Japan) instead of 10 MHz UTs were also used

for this experiment due to the lower ultrasonic propagation attenuation in the rod and water with lower ultrasonic frequencies.

Five PVC particles with known sizes supplied by CPS Instruments Inc. were used in this calibration experiment. Their optical microscope images and sizes are shown in Fig. 4.17 and Table 4-1, respectively. It should be noted that the diameter of each size standard particle has a predetermined distribution range and 90-95% of particles are in its range.

All the particles were injected through the tube with the vertical injection configuration as shown in Fig. 4.11 (b). In order to enhance the speed of data acquisition, the pulse repetition rate was set to 2500 Hz for this experiment.

Table 4-1: Specifications of five PVC particles of five known sizes used in size calibration experiment.

Mean Diameter (μm)	**Distribution Range (μm)**
82.5	70-90
98	90-106
115	105-125
137	125-150
160	150-180

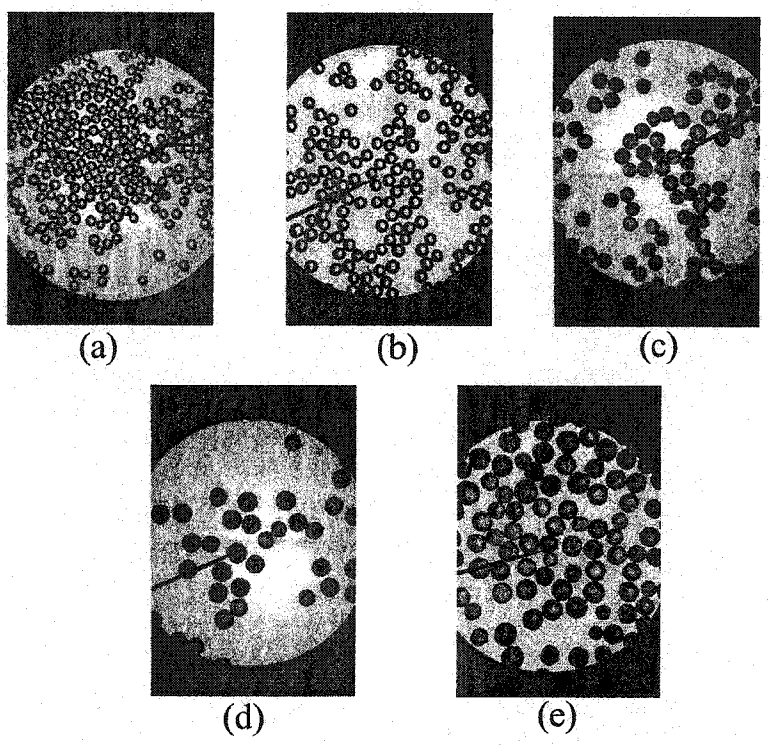

Fig. 4.17: Optical microscope images of five PVC particles used in size calibration experiment. Their mean diameters are 82.5 μm (a), 98 μm (b), 115 μm (c), 137 μm (d) and 160 μm (e).

By taking statistical analysis of the peak value of ultrasonic scattered signals, larger than noise level (0.09 V), in each particle size, mean amplitude value for each particle was determined. The results are given in Table 4-2. The standard error of the mean (*SEM*) was calculated by:

$$SEM = \frac{\sqrt{V_{ar}}}{\sqrt{n}}, \tag{4-4}$$

where $V_{ar} = \frac{1}{n-1}\sum_{i=1}^{n}(A_i - A_{av})^2$, n is the data number, A_i is the peak amplitude measured and A_{av} is the mean amplitude.

Fig. 4.18 shows the correlation between mean amplitude and mean particle diameter. The amplitude of signals monotonically increases with the particle diameter in the range of 70 to 150 μm. In the particle diameter range larger than 150 μm, the signal amplitude becomes almost constant value. Therefore, our detection sensitivity is low for the particles larger than 150 μm. The relationship between particle size and amplitude may be associated with scattering phenomena since the detected signal is the scattering ultrasound from the particles. The amplitude is associated with the value of *ka*, which is product of wave number, *k*, and particle diameter, *a*, [57]. In our experiments, *ka* is at the range from 1.474 to 3.159 for the particle diameter in the range from 70 to 150 μm at 5MHz. More theoretical investigation for ultrasonic scattering is a future study, since the detailed discussion is beyond the scope of this thesis. We drew the approximative curve manually using the measured results given in Table 4-2 by solid line as shown in Fig. 4.18. This curve represents the calibration curve from which we can determine the sizes of the particles using peak signal amplitude detected.

Table 4-2: Mean amplitude measured for different size of PVC particles in water.

Diameter(μm)	**Mean Amplitude(V)**	**SEM (V)**
82.5	0.14923	0.00216
98	0.20677	0.00364
115	0.28723	0.00542
137	0.33504	0.00587
160	0.3273	0.00623

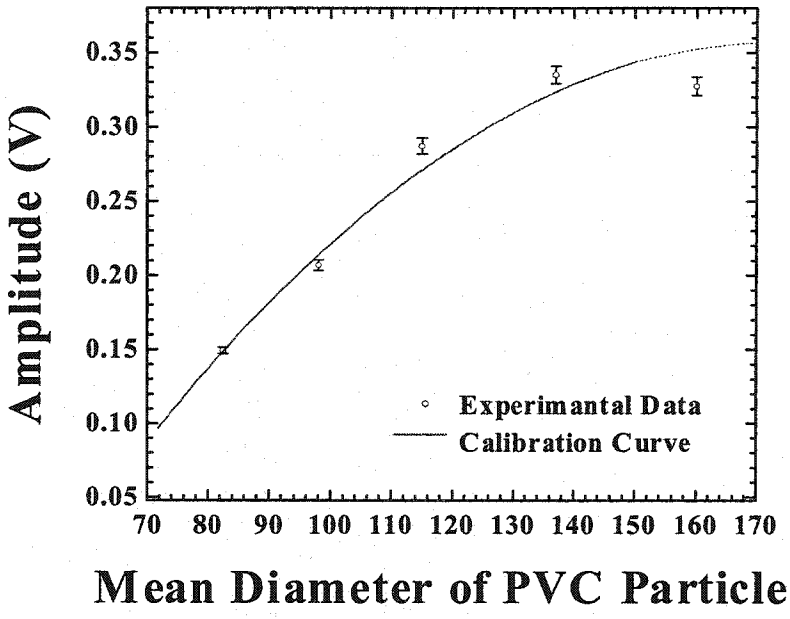

Fig. 4.18: Correlation between signal amplitude and particle size by plotting the mean average values. Solid line is the calibration curve drawn manually.

Experiment for sizing PVC particle in water was performed by mixing the four different size particles together in water tank (left) (see Fig. 4.3), in which there were about 15000 particles for each size. These numbers are estimated by measuring the weight. Through the calibration curve shown in Fig. 4.18, all peak values of the ultrasonic measured signals were converted to diameters of particles. Table 4-3 shows particle numbers counted in the different diameter ranges for 5 seconds acquisition with the flow rate, Q, of 2.16 ml/s. In the Table 4-3, the ranges of diameter of particles present the PVC particles distribution ranges for each particle. The counting error was less than 30% in all the particle diameter ranges as shown in Table 4-3.

Table 4-3: Comparison of measured number and prepared number for different size particles.

Prepared Particles			Measured Results	
Mean Diameter (μm)	Diameter Distribution (μm)	Number	Number	Error (%)
82.5	70-90	35	27	22.8
98	90-105	35	33	5.7
115	105-125	35	25	28.6
137	125-150	35	39	11.4

4.4 Summary

In this chapter, a PVC particle flow simulation system using water has been constructed in order to establish the procedure for the investigation of the optimal system configurations and for the evaluation of sensitivity, accuracy, inspection, volume, and speed, for the measurement of particle sizes, and the counting of the number of inclusions in molten metals using ultrasound. Ultrasonic probes can be installed in the system with different configurations in reflection geometries involving pulse-echo mode and pitch-catch mode.

Measuring the volume concentration of the PVC particles in water was carried out using the method presented above and the system developed with ultrasonic pitch-catch configuration at 10 MHz. It was confirmed that this ultrasonic system could differentiate different volume concentrations at 10 ppm level, even for 30 μm size of PVC particles. The linear relationship between average amplitude and concentration are obtained.

Counting the number of the PVC particles, having a mean diameter of 125 μm, suspended in water with the PVC volume concentrations of 5 ppm and 10 ppm were conducted by tube guide method with horizontal and vertical injection configurations. The ultrasonic signals scattered by the particle were detected and the particle movement was observed. The counted numbers agreed with the calculated results with a count error of less than 10%.

The size of the particles could be determined with statistical averaging of the amplitude of ultrasonic scattered signals. The correlation between amplitude and size was obtained with four different particle sizes in the range from 70 μm to 150 μm. And the error of measured numbers with prepared number was less than 30% using the calibration curve.

Chapter 5: Cleanliness Measurement for Molten Magnesium

5.1 Introduction

In this study, the methods and techniques discussed in Chapter 4 were applied to solving specific problems involving Mg. The purpose of the experiments is to detect inclusions and to evaluate relative cleanliness in molten Mg. The objective of this chapter is to perform preliminary experiments for establishing a quantitative evaluation of Mg cleanliness in the melt pool based on the results obtained from the water simulation experiments described in Chapter 4.

In recent years, the utilization of magnesium (Mg) alloys for structural applications in manufacturing, especially in the automobile industries, has been increasing rapidly. Mg alloys have the advantages of low-weight and high strength-to-weight ratios over other metals such as iron (Fe), aluminum (Al) and zinc (Zn). Processing Mg and its alloys in molten state is often necessary for refining, casting, shape forming, and recycling. In molten Mg processing, cleanliness is a crucial process parameter for part manufacturing and recycling. It is highly desirable to monitor and control the quality of the molten metals and the melting processes. However, process sensing has not been widely used due to harsh manufacturing conditions typically associated with molten Mg processes such as high temperature, corrosiveness, flammability and opaqueness.

5.2 Experimental Setup

Figure 5.1 shows the experimental setup for inclusion detection in ultrasonic pitch-catch mode. The configuration was the same as that of the particle concentration experiments using water simulation system described in Chapter 4. However, in this experiment, steel rods were chosen because of the ultrasonic wetting condition and corrosion of the probe in molten Mg as mentioned in Chapter 1. When the steel rod is immersed into the molten Mg, the ultrasonic transmission coefficient at the interface between steel and molten Mg is 0.35, which is higher than that between Al and water as mentioned in Chapter 4. In addition, in order to improve the sensitivity of the inclusion detection, the double-taper shape clad steel buffer rods were used here due to the fact that they have a higher SNR over the non-clad ones [31,40,44]. A detailed design of the rods such as taper angle and the rod evaluation can be found in literature [47]. Fig. 5.2 shows a double-taper shape clad steel buffer rod, consisting of a mild steel core and stainless steel (SS) cladding, used in the experiment. The SS cladding was fabricated outside of the steel core by the thermal spray technique. The dimensions of the rod are as follows: the length is 258 mm with taper angle of 2°, the diameters at the middle and at the ends are 23.4 mm and 13.2 mm, respectively, and the thickness of the cladding is about 1mm.

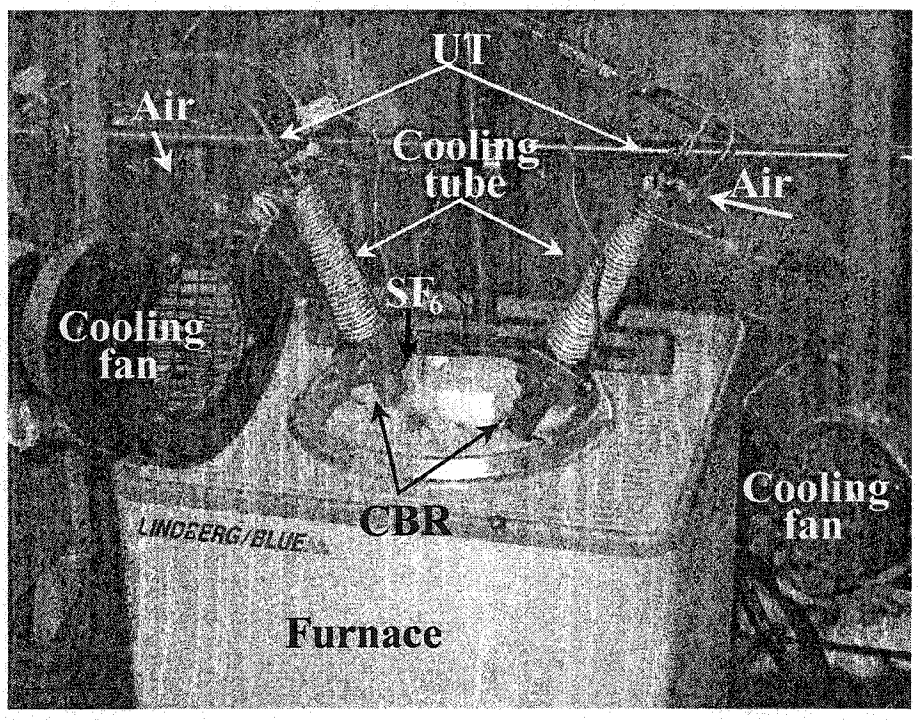

Fig. 5.1: Experimental setup for inclusion detection in molten Mg with ultrasonic pitch-catch configuration.

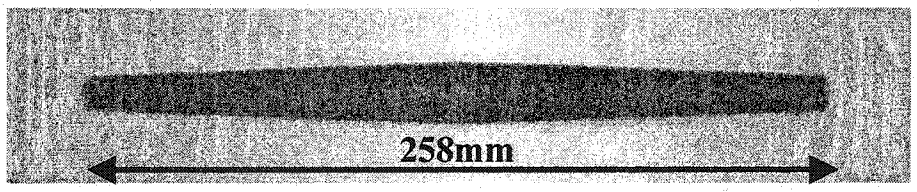

Fig. 5.2: Double-taper shape clad steel buffer rod having the length of 258mm used for ultrasonic probe.

Throughout the experiment, longitudinal wave ultrasonic transducers with a center frequency of 10MHz were used. Because of the high temperature conditions, an air cooling system was attached to the UT ends to protect the UTs. Pure Mg (Purity: 99.80%, Timminco Ltd., ON, Canada) contained in a SS crucible was heated by an

electric resistance furnace (Model: CF 56822C, Lindberg/Blue M, USA). The temperature of the molten Mg was measured by a thermocouple immersed in the molten Mg. SF_6 gas was continually supplied above the surface of the molten Mg to avoid oxidation and burning of the molten Mg since the molten Mg is reactive with oxygen and ignites in the atmosphere [14, 71-72]. The dimensions of the crucible were 90 mm in diameter and 100 mm in depth, and the depth of the molten Mg was approximately 70 mm. The sensing area was located at the center of the crucible. The center of the crucible was about 30 mm below the surface of the molten Mg.

5.3 Experimental Results

5.3.1 Particle Detection

As discussed in Chapter 1, the composition of inclusions in magnesium is complicated. In this experiment, the origins of the inclusions would be from Mg itself and those created on the surface of molten Mg with the protective gas SF_6. Because the inclusions, had different densities and were either heavier or lighter than molten Mg, some settled to the bottom and some were suspended on the surface. In order to detect inclusions in the molten Mg, the molten Mg was manually stirred to distribute the present inclusions uniformly in the molten Mg before acquiring the signals. Although a few signals, probably from the inclusions, were already observed before the stirring process due to convection of molten Mg. A typical result is shown in Fig. 5.3. With the temperature of the molten Mg at 680°C, the backscattered ultrasonic signals from the inclusions were

successfully observed when the inclusions were passing through the sensing area. Movements of the inclusions were visible. The signals were recorded every 2 msec with a time window of 20 μsec covering the whole sensing area, and all the desired signals reflected from the inclusions were in this window. Here only the frames at an interval of 10 msec with a time window of 6 μsec are shown in Fig. 5.3. The echoes from the inclusions appeared in the time delay range from 92 to 112 μsec with the presented experimental conditions. The time delay range of the signals appearing depends on the probe dimensions such as length and diameter, and configurations such as distance and angle between two probes. The inclusions detected might be oxides, metallic particles and/or protective films in the molten Mg [11-14]. The magnesium oxide was created by the reaction of the molten Mg with air even though SF_6 gas was supplied to prevent oxidation.

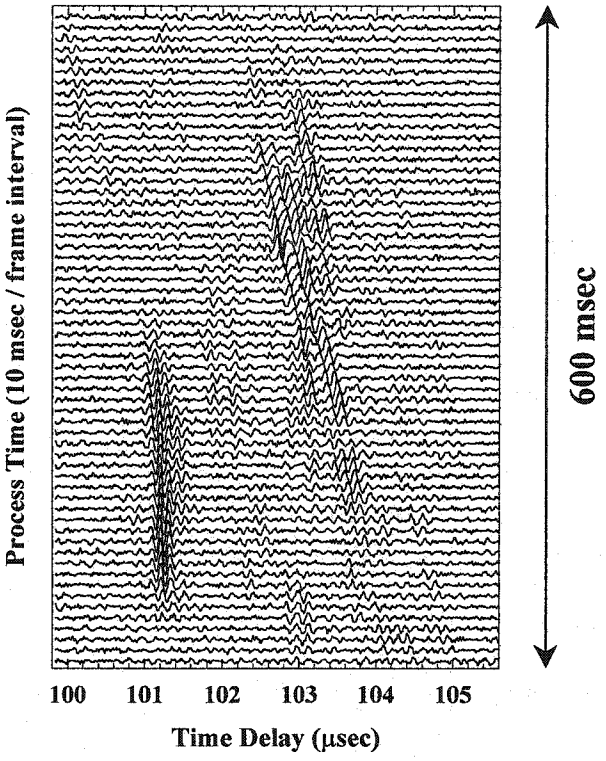

Fig. 5.3: Typical detected backscattered signals from inclusions in molten Mg at 680^0C operated at 10 MHz.

5.3.2 Relative Cleanliness Measurement

It has been proven that the clad steel buffer rods are capable of detecting inclusions in molten Mg as discussed in the previous section. However, since the movements of the inclusions were random in the melts under the experimental conditions, it is difficult to determine the size and the number of the inclusions in the melts using the signals shown in Fig. 5.3. Here, relative cleanliness evaluations of the molten Mg can still be investigated using the signals obtained with the measurement configuration shown in Fig. 5.1.

Figure 5.4 shows the signals obtained for a period of 5 seconds at each measurement time of 0 sec (a), 140 sec (b), 280 sec (c), and 580 sec (d) after stirring of the molten Mg. Many signals from inclusions were observed just after the stirring as seen in Fig 5-4 (a). However the number and the amplitude of the signals gradually decreased as the measurement time continued, since the inclusions were heavier or lighter than the molten Mg, and they settled to the bottom or top of the melt. In this case, less and smaller inclusions passed through the sensing area located at the center of the melt in this experiment.

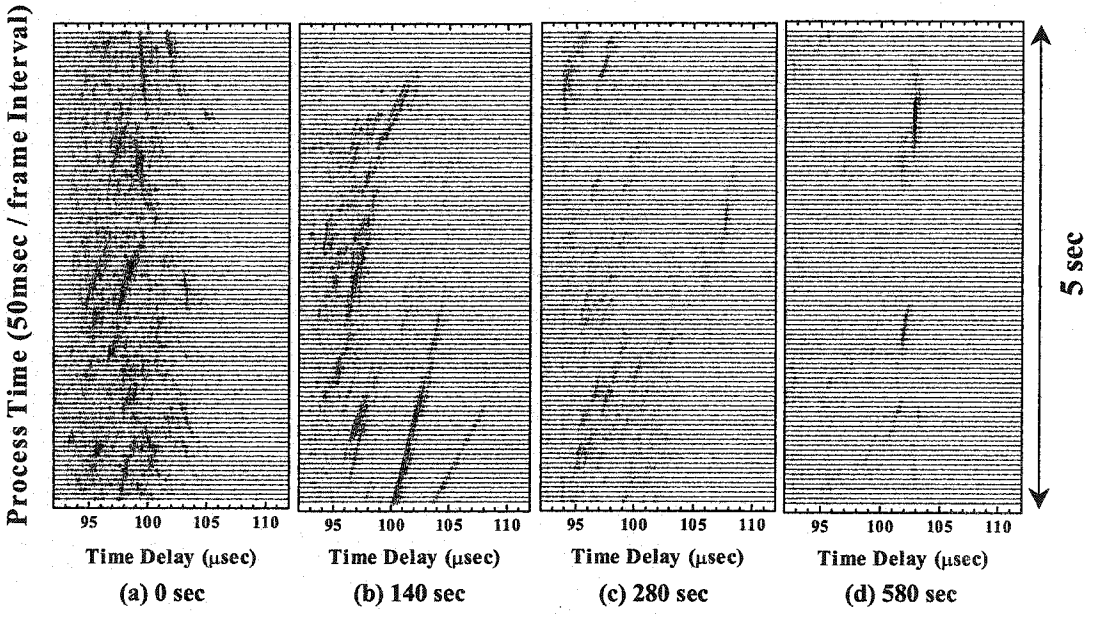

Fig. 5.4: The signals obtained for a period of 5 seconds at each measurement time of 0sec (a) 140sec (b) 280sec (c) and 580sec (d) after stirring of molten Mg.

A histogram shown in Fig. 5.5 presents the variations of the total power of the signals with respect to the measurement time. The total power that was obtained by the

summation of the power of detected signals appearing in the time delay, ranges from 92 to 112 μsec during 5 seconds acquisition in each 20 seconds. The temperature range was between 690 and 700°C for all the experiments. Just after stirring molten Mg, the detected power was the largest at 0 sec, then, it gradually decreased with respect to the measurement time as predicted. The arrows shown in the figure correspond to the power obtained from the signals shown in Fig. 5.4. At the measurement time of 590 seconds, the second stirring of molten Mg was performed and one can see that the detected power increased again. As shown in Fig. 5.5, the inclusion distribution (cleanliness) in the melt pool can be evaluated by moving the probes to different depths in the molten Mg instead of stirring the melt. Dirty melts scatter back more ultrasound than clean melts. By examining the relative cleanliness distribution in melt pool, one can know that area and volume of the melt which has acceptable cleanliness for manufacturing products.

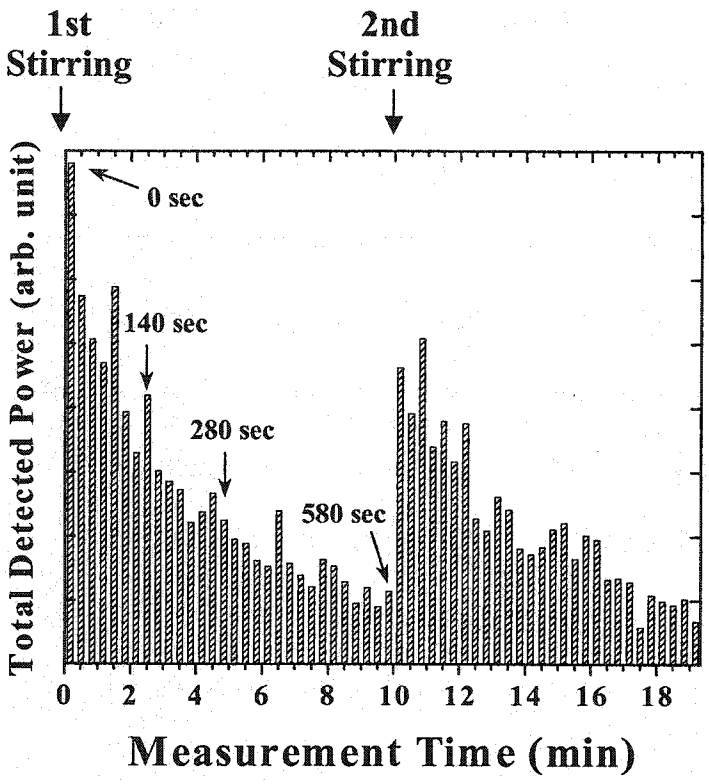

Fig. 5.5: Variation of total power of the detected signals in molten Mg with respect to a measurement time after stirring.

5.4 Summary

Based on the results obtained from water simulation experiments for particle concentration measurements, this chapter demonstrates the capability of ultrasonic techniques for the relative cleanliness evaluation in molten Mg using clad steel buffer rods operated at 10 MHz. The ultrasonic signals scattered from the inclusions in the molten Mg at 680°C were successfully observed. The movements of the inclusions were visible in the pitch-catch mode using the plane waves due to the high SNR of the clad

steel buffer rods. This system is able to provide relevant information on inclusion concentration.

Since the movements of the inclusions were random in the molten Mg under these experimental conditions, it is difficult to determine the size and the number of the inclusions from the signals obtained in this experiment. Although the details of the inclusions such as the size and the number are not yet known at this moment, they could be determined by controlling the inclusion movement and speed using a tube and a molten metal pump as verified by the water simulation experiments described in Chapter 4. Our future study will develop the quantitative evaluation of the metal cleanliness by measuring the size and counting the number of inclusions.

Chapter 6: Conclusions

6.1 Thesis Review

In this thesis, the water simulation system including ultrasonic probes, configuration of electronics and PVC particles in water has been designed, constructed and tested in order to establish the procedure and to investigate the optimum sensors , technique and system configurations for cleanliness evaluation of molten metals.

In chapter 2, basic ultrasonic concepts such as SNR, the reflection and transmission coefficients, attenuation and scattering signals were illustrated. The pitch-catch ultrasonic measurement configuration was used since this configuration can effectively avoid spurious echoes overlapping the desired echo (L^1) during particle detection. The data acquisition system, including the hardware and software mainly used in this thesis, was introduced. The fastest speed of data recording achieved was 1/3 ms per frame, which enable us to detect particle movements in the sensing area precisely.

In chapter 3, the ultrasonic performance of several materials and three different cross-section shapes of metallic buffer rods with cladding or non-cladding and UTs with circular and square shapes were investigated experimentally. Among commercially available aluminum, titanium, magnesium and mild steel, it was found that a mild steel rod with fine grains provided a strong signal strength and a high SNR in pulse-echo technique. High SNR can make many practical ultrasonic applications feasible. The

non-clad Al rods were used to study the effects of the shapes of the rods on the SNR. The overall best SNR of 36 dB in signal L^1 was achieved with a combination of the circular rod and the square UT. The SNR of more than 40 dB in L^1 was achieved for all the cladding rods consisting of a metallic core and stainless steel cladding fabricated by a thermal spray method. Furthermore, UFD experiments showed that the ultrasound radiated in water from the probing end was in far-field region and the shape of the ultrasound beam was the same as the rod shape. It was also found that the circular rod had a larger beam width than the square rod and 5 MHz UT would offer larger sensing area than 10 MHz UT.

In chapter 4, the water simulation system of ultrasonic detection particles was constructed, in which measuring concentration, counting the number and measuring the size distribution of the PVC particles were performed with the pitch-catch configuration. It was confirmed that this ultrasonic system could differentiate concentrations of inclusions at 10 ppm level, even for 30 μm size PVC particles in water. A linear relationship of average amplitude of ultrasonic signals and particle concentration was found. Through using a tube to guide particle movement to ensure that only one particle passed through the sensing area at one time, the ultrasonic signals scattered by each single particle were detected and the particle movement was observed. The number of the PVC particles with a mean diameter of 125 μm, suspended in water with the volume concentration of 5 ppm and 10 ppm, was counted. And the counted numbers agreed with the calculated results within a count error of less than 10% or two counts. Furthermore, the relationship between the scattered signal amplitude and the particle size was

investigated by using PVC particles of known size. The size of the particles, at the range of 70 to 150 μm, could be determined by their scattered signal amplitude with a counting error less than 30%. But for the particles larger than 150 μm, our detection sensitivity is low, which will be investigated in the future.

In chapter 5, the capability of the ultrasonic detection system developed in the water simulation of chapter 4, was tested in molten magnesium in the lab. The backscattered signals from the inclusions in molten Mg at 680 ^{0}C were successfully observed and movements of inclusions were visible by using clad steel buffer rods operated at 10 MHz. Since the movements of the inclusions were random under presented experimental conditions, it was difficult to provide further details about the inclusions.

6.2 Original Contributions

This research has introduced several original contributions that are summarized below:

(1) We have designed three different cross-section shaped rods and investigated their SNR with circle and square UT experimentally. It has been proven that a 36 dB SNR could be obtained using the non-clad rod. It is well known that cladding rods have high SNR, but non-cladding rods are of low cost. It is the first report in which the square cross-section shape of rods can be used in cleanliness evaluations. Details can be found in reference [70].

(2) We utilized the technique involving the scanning of a small ball bearing immersed in water as an ultrasonic target in the pitch-catch mode to investigate UFD. Satisfactory images of ultrasonic wave patterns near the probe end in the water were obtained.

(3) We successfully constructed the water simulation system for ultrasonic detection of particles. This system can be used to measure concentrations, count the number, and measure the size distribution of the PVC particles in the water. The sensing configuration can differentiate between concentrations of inclusions at 10 ppm step for 30 μm size PVC particles. The error for counting the number of particles in water is less than 10%. The measured size for a single PVC particle was as small as 82.5 μm. Details can be found in reference [73-74].

6.3 Future Work

As mentioned in Chapter 1, ultrasonic probes are crucial for the ultrasonic cleanliness evaluation system. In Chapter 3, it was found that the combination of a square cross-section rod with a circular UT or that of a circular cross-section rod with a square UT had the highest SNR among all the combinations of these three different shaped rods and two shapes of UTs. However, in our calibration experiments, we used square cross-section rods with square UTs because we didn't have two circular 5 MHz UTs at that moment. Fig. 3.11 showed that the circular cross-section rods had a larger strong signal area than

square cross-section rods. Therefore, we suggest testing the circular cross-section rod with the square UT in a future study.

It was also observed that the amplitude of scattered echoes was not constant even for the standard PVC particles. The reasons could be: (1) each PVC particle did not pass through the exact sensing center; (2) the size and shape of the calibration PVC particles was not uniform and (3) scattering echoes were complicated. Therefore, we suggest choosing a tube with a small diameter and setting it closer to the sensing center of the probes. Selecting uniform particles for further calibration is necessary in the future.

Furthermore, the relationship between particle size and ultrasonic signal amplitude may be explained by introducing scattering theory. Only the amplitude of backscattered signal is used here to measure the size of the particle. Fast Fourier Transform (FFT) analysis may give some information about particle size and shape. Therefore, scattering theories and FFT analysis should be further researched in the future.

REFERENCES

[1] P. Hauptmann, N. Hoppe and A. Puttmer, "Application of ultrasonic sensors in the process industry," Measurement Science and Technology, pp. R73-R83, July, 2002.

[2] R. S. Young and D. E. Pitcher, "Method of and apparatus for testing molten metals," US Patent 3,444,726, 1969.

[3] T. L. Mansfield, "Probe for the ultrasonic inspection of molten aluminum," US Patent 4,261,197, 1981.

[4] T. L. Mansfield, "Probe for the ultrasonic treatment or inspection of molten aluminum, probes for use in such testing," US Patent 4,287,755, 1981.

[5] C. E. Eckert, "Apparatus and method for ultrasonic detection of inclusions in molten metals," US Patent 4,563,895, 1986.

[6] N. D. G. Mountford, "Testing of liquid melts and probes for use in such testing," US Patent 4,981,045, 1991.

[7] N. D. G. Mountford and I. D. Sommerville, "Ultrasonic detection techniques," US Patent 5,604,301, 1997.

[8] R. C. Stiffler, R. C. Wojnar, M. F. A. Warchol, L.W.Cisko, and J.M.Urbanic, "Apparatus and method for ultrasonic particle detection in molten metals," US Patent 5,708,209, 1998.

[9] W. P. Peterson, "The role of casting technology in the development of new and improved fabricated products," Light Metals, pp. 329-339, 1988.

[10] P. N. Crepeau, "Molten aluminum contamination: gas, inclusions and dross," Modern Casting, Vol. 87, pp. 39-41, 1997.

[11] D. Oymo, D. O. Karlsen, P. M. D. Pinfold, T. Mellerud, and O. Lie, "Particle removal in pure magnesium," Light Metals, Ed. U. Mannweiler, The Minerals, Metals & Materials Society, pp. 1017-1024, 1994.

[12] H. Hu and A. Luo, "Inclusions in molten magnesium and potential assessment techniques," J.O.M., pp. 47-51, Oct. 1996.

[13] C. J. Simensen and B. Oberländer, "A survey of inclusions in magnesium," Praktische Metallographie, Vol. 17, pp. 125-136, 1980.

[14] S. P. Cashion, N. J. Ricketts, and P .C. Hayes, "The mechanism of protection of molten magnesium by cover gas mixtures containing sulphur hexafluoride," Light Metals, pp. 43-47, 2002.

[15] I. D. Sommerville, N. D. G. Mountford, and L. C. B. Martines, "Laboratory and industrial validation of an ultrasonic sensor for cleanliness measurement in liquid metals," Light Metals 2000, R. D. Peterson Ed. Warrendale, PA: The Minerals, Metals & Materials Society, pp. 721-726, 2000.

[16] D. A. Doutre and R. I. L. Guthrie, "Method and apparatus for the detection and measurement of particles in molten metal," US Patent 4555662, 1985.

[17] R. I. L. Guthrie, "Molten metal inclusion sensor probe," U.S. Patent, 5,789,910, 1998.

[18] C. Dupuis, F. Dalllaire and B. Maltais, "The measurement of controlled size particles in molten aluminum using the LiMCA II technique," Bomen Inc.

[19] R. I. L. Guthrie, M. Isac, M. Li, and J. Y. Byun, "An on-line system for the detection of inclusions in molten magnesium based on the electric sensing zone principle," in Proc. 1st Israeli Int. Conf. on Magnesium Science and Technology, pp. 81-87, Nov. 1997.

[20] R. I. L. Guthrie and M. Li," In Situ detection of inclusions in liquid metals: part I. mathematical modeling of the behavior of particles traversing the electric sensing zone," Metallurgical and Materials Transactions B, 32B, pp. 1067-1079, Dec. 2001.

[21] R. I. L. Guthrie and D. A. Doutre, "On-line measurements of inclusions in liquid metals," International Seminar on Refining and Alloying of Liquid Aluminum and Ferro-Alloys, 147-163, 1985.

[22] N. D. G. Mountford et al., "Precipitation effects in liquid aluminum alloys: experiments with pulsed ultrasonic technique," Journal of Institute of Metals, vol. 88, 121-127, 1959-1960.

[23] T. L. Mansfield, "Ultrasonic technology for measuring molten aluminum quality," Materials Evaluation, vol. 41, 743-747, 1983.

[24] T. L. Mansfield, "Molten metal quality measured with Reynolds 4MTM system," Light Metals, pp. 1305-1327, 1984.

[25] N. D. G. Mountford, A. Simionescu, and I. D. Sommerville, "Visualization of the particle content of liquid aluminum alloys," Light Metals 1997, Ed. R. Huglen, The Minerals, Metals & Materials Society, pp. 937-943, 1997.

[26] N. D. G. Mountford, I. D. Sommerville, A. Simionescu, and C. Bai, "Sound pulses used for on-line visualization of liquid metal quality," AFS Transactions, Vol. 105, pp. 939-946, 1997.

[27] N. D. G. Mountford et al., "A measurement device for quality control in liquid metals," Proc. 6th international conference on refining process, Lulea, Sweden, 465-488, 1992.

[28] P. Hauptmann, Niels Hoppe, and A. Pütter, "Application of ultrasonic sensors in the process industry," Measurement Society Technology, Vol. 13, pp. R73-R83, 2002.

[29] N. D. G. Mountford et al., "The relationship between inclusion contents as measured by ultrasonic testing in liquid steel and cast metal quality," Process Electric Furnace Conference, Iron and Steel Society, AIME, vol. 49, 243-248, 1991.

[30] C. K. Jen, "Acoustic fibers," Process IEEE Ultrasonics Symposium. 87CH24927, 443-454, 1987.

[31] C.-K. Jen and J.-G. Legoux, "Clad ultrasonic waveguides with reduced trailing echoes," US Patent 5,828,274, 1998.

[32] C.-K. Jen, L. Piche, and J. F. Bussiere, "Long isotropic buffer rods," Journal of Acoustic Society, America, Vol. 88, No. 1, pp. 23-25, July 1990.

[33] H. Karasawa, M. Izumi, T. Suzuki, A. Nagai, M. Tamura, and S. Fujimori, "Development of under-sodium three-dimensional visual inspection technique using matrix-arrayed ultrasonic transducer," Journal Nuclear Science and Technology, Vol. 37, No. 9, pp. 769-779, Sept. 2000.

[34] D. I. Walker, S. Dawson, N. D. G. Mountford, I. D. Sommerville, and A. McLean, "The development of ultrasonic sensors for the early detection of slag carryover," Transaction of the Iron and Steel Society, Vol. 12, pp. 223-230, 1991.

[35] J. -F. Moisan, C.-K. Jen, J.-W. Liaw, C.-Q. Zheng, T.-F. Chen, Z. Sun, and C. A. Loong, "Ultrasonic sensor and technique for on-line monitoring of die casitng process," Measurement Science Technology, Vol. 12, pp. 1956-1963, 2001.

[36] C.-K. Jen, J.-F.Moisan , C.-Q, Zheng, C.A. Loong, S.E.Kruger,M.T. Shebata and E. Essadiqi, "Ultrasonic characterization and monitoring of semi-solid magnesium die casting process," 7th International Conference on Semi-solid Processing of Alloys and Composites, 2002.

[37] C.-K. Jen, D. R. França, A. Sun, and I. Ihara, "Clad polymer buffer rods for polymer process monitoring," Ultrasonics, Vol. 39, pp. 81-89, 2001.

[38] S.-S. L. Wen, C.-K. Jen, and K. T. Nguyen, "Advances in on-line monitoring of the injection molding process using ultrasonic techniques," International Polymer Processing XIV, 175-182, 1999.

[39] D. R. França, C.-K. Jen, K.T. Nguyen, and R. Gendran, "Ultrasonic in-line monitoring of polymer extrusion," Polymer Engineering and Science, Vol. 40, pp. 82-94, 2000.

[40] C.-K. Jen and N. Legros, "High performance clad metallic buffer rods," Process IEEE Ultrasonic Symposium, 771-776, 1996.

[41] J.-G. Legoux and C.-K. Jen, "Ultrasonic applications of thick metallic coatings," in Process 9th National Thermal Spray Conference, pp.65-72, 1996.

[42] F. A. Lowenheim, *Modern Electroplating*, (New York: John Wiley and Sons, 3rd Edition, 1974).

[43] Y. Ono, J.-F. Moisan, C.-K. Jen and D. R. Franca, "Development of ultrasonic techniques with buffer rod in molten aluminum," To appear in the 2002 IEEE International Ultrasonics Symposium, Munich, Germany, Oct. 2002.

[44] C.-K. Jen, J.-G. Legoux, and L. Parent, "Experimental evaluation of clad metallic buffer rods for high temperature measurements," Nondestructive Test Evaluation. International, Vol. 33, pp. 145-153, 2000.

[45] I. Ihara, C.-K. Jen, and D. R. França, "Material evaluation using long clad buffer rods," in Process IEEE Ultrasonic Symposium, pp. 803-807, 1998.

[46] I. Ihara, C.-K. Jen, and D. R. França, "Detection of inclusion in molten metal by focused ultrasonic wave," Japanese Journal Application Physics, Vol. 39, Part 1, No. 5B, pp. 3152-3153, May 2000.

[47] I. Ihara, C.-K. Jen, and D. R. França, "Materials evaluation in molten metal using focused ultrasonic sensors: application to molten zinc," the 2nd international symposium, Asian, Korea, ATM, Vol. 3, pp. 45-50, February, 2001.

[48] D. Pierre, F. Bosselet, M. Peronnet, J. C. Viala and J. Bouix, "Chemical reactivity of iron base substrates with liquid Mg-Zr alloys," Acta Material, Vol. 49 653–662, 2001.

[49] A. Molinari, M. Pellizzari, G. Straffelini, and M. Pirovano, "Corrosion behaviour of a surface-treated AISI H11 hot work tool steel in molten Aluminium alloy," Surface and Coatings Technology, 126, 31-38, 2000.

[50] H.-N. Ho and S.-T. Wu, "The wettability of molten aluminum on sintered aluminum nitride substrate," Material Science and Engineering, A248, 120-124, 1998.

[51] I. Ihara, C.-K. Jen, and D. R. França, "Ultrasonic imaging, particle detection, and V(z) measurements in molten zinc using focused clad buffer rods," Review of Scientific Instruments, Vol. 71, No. 9, pp. 3579-3586, Sept. 2000.

[52] I. Ihara, C.-K. Jen, and D. R. França, "C-scan imaging in molten zinc by focused ultrasonic waves," Journal Acoustics Society American, Vol. 107, No. 2, pp. 1042-1043, Feb. 2000.

[53] L. C. Lynnworth, *Ultrasonic Measurements for Process Control* (New York: Academic, 1989).

[54] R. Redwood, *Mechanical Waveguides* (New York: Pergamon, 1960), Chap. 9, pp. 191-207.

[55] L. E. Kinsler, A. R. Frey, A. B. Coppens, and J. V. Sanders, *Fundamentals of Acoustics* (New York: John Wiley & Sons, 3rd Edition,1982).

[56] B. M. Lempriere, *Ultrasound and Elastic Waves-Frequently Asked Questions* (New York: Academic Press 2002), pp. 61-63.

[57] R. Truell, C. Elbaum and B. B. Chick, *Ultrasonic Methods in Solid State Physics* (New York: Academic Press 1969), pp. 161-180.

[58] J. J. Faran, "Sound scattering by solid cylinders and spheres," Journal Acoustics Society American, Vol. 23, No. 4, pp. 405-418, July 1951.

[59] A. Briggs, *Acoustic microscopy* (Oxford: Clarendon, 1992), pp. 102-103.

[60] J. T. McElroy, "Identification and measurement of ultrasonic search unit characteristics," Materials Evaluation, Vol. 25, No. 6, pp. 129-137, 1967.

[61] E. P. Papadakis and K. A. Fowler, "Broad-band transducers: radiation field and selected applications," Journal Acoustics Society American, Vol. 50, No. 3, pp. 729-745, 1971.

[62] P. G. Kenny, J. J. Gruber and J. M. Smith, "Ultrasonic transducer characterization," Materials Evaluation, Vol. 45, pp. 730-735, 1987.

[63] D. R. Franca, C.-K. Jen and I. Ihara, "Ultrasonic fields of clad buffer rods imaging probes," Process International Acoustical Imaging Symposium, pp. 443-452, 2001.

[64] G. R. Harris, "Hydrophone measurements in diagnostic ultrasound fields," IEEE Transactions on Ultrasonic, Ferroelectrics, and Frequency Control, Vol. 35, No. 2, pp. 87-101, 1988.

[65] T. M. Mansour, "Evaluation of ultrasonic transducers by cross-sectional mapping of the near field using a point reflector," Materials Evaluation, Vol. 37, No. 7, pp. 50-54, 1979.

[66] K. Raum and W. D. O'Brien, "Pulse-echo field distribution measurement technique for high-frequency ultrasound sources," IEEE Translations on Ultrasonic, Ferroelectrics and Frequency Control, Vol. 44, No. 4, pp. 810-815, 1997.

[67] G. S. Kino, *Acoustic Waves: Devices, Imagine, and Analog Signal Processing* (Englewood Cliffs: Prentice-Hall, 1987), Chapter 3, pp. 154-317.

[68] W. Kroebel and K.-H. Mahrt, "Recent results of absolute sound velocity measurements in pure water and sea water at atmospheric pressure," Acoustics, Vol. 35, pp. 154-164, 1976.

[69] S. P. McAlister, E. D. Crozier and J. F. Cochran, "Sound velocity and compressibility in the liquid alkaline earth metals," Canadian Journal Physics, Vol. 52, pp. 1847-1851, 1974.

[70] Y. Ono, Y. Zhang, C.-K. Jen, J.-F. Moisan, J.-G. Gegoux and C.-Y. Su, "Metallic buffer rods for ultrasonic monitoring of industrial material processes,"(Paper presented in the 4th International Conference on Industrial Automation, Montreal, Canada, June 9-11, 2003), Paper No. INS-05.

[71] C. S. Roberts, *Magnesium and its alloys*, (New York: John Wiley & Sons, 1960).

[72] F. Czerwinski, "The oxidation behaviour of an AZ91D magnesium alloy at high temperatures," Acta Material, Vol. 50, pp. 2639-2654, 2002.

[73] Y. Ono, Y. Zhang, J.-F. Moisan, C.-K. Jen, and C.-Y. Su, "Simulation experiments in water for ultrasonic detection of inclusions in molten metals,"(Paper presented in the 4th International Conference on Control and Automation, Montreal, Canada, June 9-12, 2003).

[74] Y. Ono, J.-F. Moisan, Y. Zhang, C.-K. Jen, and C.-Y. Su, "Ultrasonic inclusion detection and cleanliness measurement in molten aluminum and magnesium,"(Paper presented in the 2003 Fall Meeting of the Minerals, Metals &

Materials Society and the 45th Iron &Steel Society Mechanical Working and Steel Processing Conference, Chicago, U.S., November 9-12, 2003).